THE ASTROPHYSICAL JOURNAL, 470:172–188, 1996 October 10

THE LAS CAMPANAS REDSHIFT SURVEY

STEPHEN A. SHECTMAN AND STEPHEN D. LANDY
Carnegie Observatories, 813 Santa Barbara Street, Pasadena, CA 91101; shec@ociw.edu, landy@ociw.edu
AUGUSTUS OEMLER
Department of Astronomy, Yale University, New Haven, CT 06520-8101; oemler@astro.yale.edu
DOUGLAS L. TUCKER
Astrophysikalisches Institut Potsdam, An der Sternwarte 16, D-14482 Potsdam, Germany; dtucker@aip.de
HUAN LIN[1] AND ROBERT P. KIRSHNER
Harvard-Smithsonian Center for Astrophysics, 60 Garden Street, Cambridge, MA 02138;
hlin@cfa.harvard.edu, kirshner@cfa.harvard.edu
AND
PAUL L. SCHECHTER
Department of Physics, Massachusetts Institute of Technology, Cambridge, MA 02139; schech@achernar.mit.edu
Received 1995 December 28; accepted 1996 April 30

ABSTRACT

The Las Campanas Redshift Survey (LCRS) consists of 26,418 redshifts of galaxies selected from a CCD-based catalog obtained in the R band. The survey covers over 700 deg^2 in six strips, each 1°.5 × 80°, three each in the north and south Galactic caps. The median redshift in the survey is about 30,000 km s^{-1}. Essential features of the galaxy selection and redshift measurement methods are described and tabulated here. These details are important for subsequent analysis of the LCRS data. Two-dimensional representations of the redshift distributions reveal many repetitions of voids, on the scale of about 5000 km s^{-1}, sharply bounded by large walls of galaxies as seen in nearby surveys. Statistical investigations of the mean galaxy properties and of clustering on the large scale are reported elsewhere. These include studies of the luminosity function, power spectrum in two and three dimensions, correlation function, pairwise velocity distribution, identification of large-scale structures, and a group catalog. The LCRS redshift catalog will be made available to interested investigators at an internet web site and in archival form as an AAS CD-ROM.

Subject headings: cosmology: observations — galaxies: clusters: general — galaxies: distances and redshifts — surveys

1. INTRODUCTION

Redshift surveys reveal surprising structures in the large-scale distribution of galaxies which provide clues to physical properties of the universe (see Giovanelli & Haynes 1991 and Strauss & Willick 1995 for reviews). Early investigations (such as Kirshner et al. 1981 or Huchra et al. 1983) suggested that the nearby universe might be strongly inhomogeneous with nearly empty voids and thin, high contrast regions of galaxy overdensity. Convincing demonstrations that this pattern is a general feature of the universe have come from extensive surveys which cover large angles on the sky (for summaries of the CfA surveys, see de Lapparent et al. 1986 and Geller & Huchra 1989; for the Southern Sky Redshift Survey, see da Costa et al. 1994a). Galaxies appear to lie on networks of filaments or sheets extending over 100 h^{-1} Mpc that encompass sharply bounded voids (Hubble constant $H_0 = 100\,h$ km s^{-1} Mpc^{-1}). Despite the power of the CfA2 (Huchra et al. 1996) and the Southern Sky Redshift Survey (SSRS2) in conveying an impression of the galaxy distribution on large scales, the largest features they reveal are very near the upper limit set by the depth of the survey at about 12,000 km s^{-1}.

Are these the largest features in the universe? There are hints of possible structure on larger scales from apparent periodicities in redshifts (Broadhurst et al. 1990), from the flows suggested by Lauer & Postman (1994), or from possible variations in the luminosity density (da Costa et al. 1994a). Only a deep extensive survey can provide evidence on the reality of these suggestions. Similarly, the statistical measures of galaxy clustering derived from redshift catalogs (Efstathiou 1993; Park et al. 1994), which can be used to constrain models for the formation of structure in the universe, have only modest precision at the large scales which are most interesting. To explore structure in the local universe on a scale of 30,000 km s^{-1} and to improve our measures of galaxy statistics, we have been working since 1987 on the Las Campanas Redshift Survey (LCRS). We have compiled a CCD-based galaxy catalog, selected the galaxies, developed the fiber-optic equipment for mass producing galaxy spectra, and observed from 1988 to 1994. We have measured more than 26,000 galaxy redshifts averaging $z = 0.1$ over an area of 700 deg^2 arranged in six long thin strips, three in the north Galactic cap and three in the south. The LCRS provides a reconaissance of present-day structure on the largest scales mapped to date.

The LCRS is a direct descendent of earlier surveys aimed at measuring the average properties of galaxies: the luminosity function and the space density of galaxies (Kirshner et al. 1978, 1979, 1983). Annoying variations in the average properties, such as the luminosity density, signaled the presence of strong inhomogeneities in the galaxy distribution. Most startling was a large void of diameter 60 h^{-1} Mpc in

[1] Present affiliation: Department of Astronomy, University of Toronto, 60 Saint George Street, Toronto, ON, Canada M5S 3H8; lin@astro.utoronto.ca.

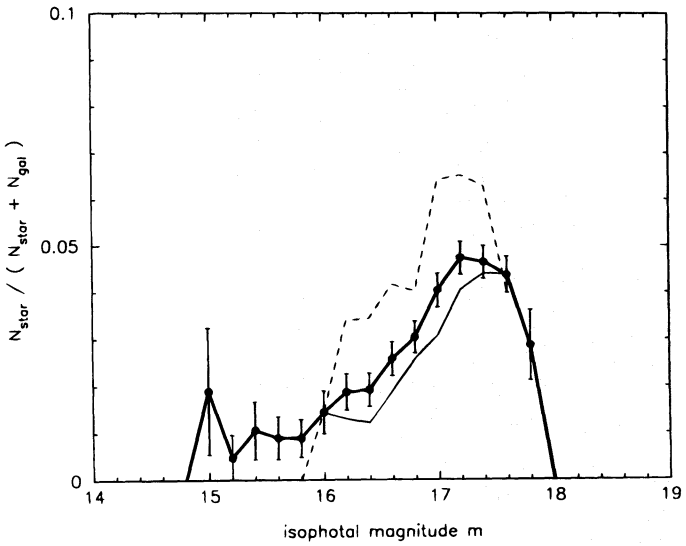

FIG. 1a

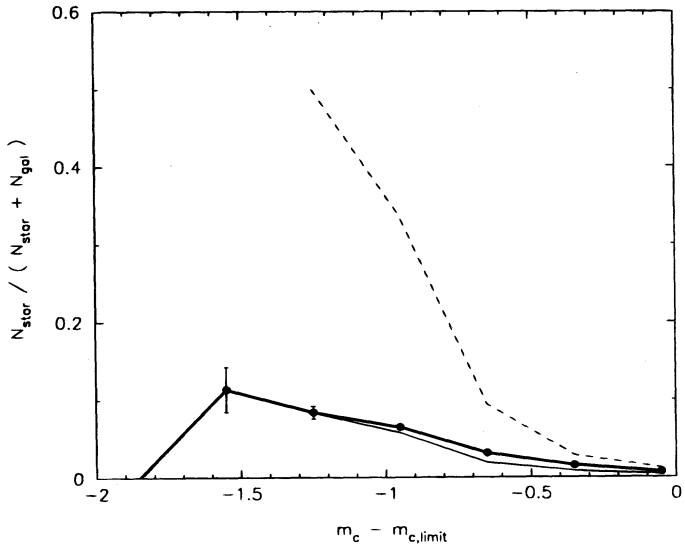

FIG. 1b

FIG. 1.—Ratio $N_{star}/(N_{star} + N_{gal})$ (*a*) vs. isophotal magnitude and (*b*) vs. distance $m_c - m_{c,limit}$ from the central surface brightness "cut line," where $m_{c,limit} \equiv m_{cen} - 0.5(m_2 - m)$. Here m_{cen} and m_2 are the proper values for an object within a given field and are taken from Table 2. In both plots, the filled circles connected by the thick solid line denote the ratio for the full LCRS sample; the dashed line, the 50 fiber sample; and the thin solid line, the 112 fiber sample. Note that in (*b*) the high value of the ratio for the 50 fiber sample at $m_c - m_{c,limit} = -1.25$, is due to just two objects: one star and one galaxy. Poisson errors are shown.

the galaxy distribution beyond the constellation Boötes (Kirshner et al. 1981, 1987, 1990). Because similar structures are now frequently seen in wider angle surveys and because the structures are nearly as large as the survey dimensions, a much larger and deeper survey seems needed in order to encompass a fair sample of the universe, as well as to search for structure on larger scales. The LCRS began with a goal of obtaining a galaxy sample of sufficient size, sky coverage, and depth to permit a reliable characterization of the average properties of galaxies and of their distribution.

While this work was in progress, some important large wide-angle redshift surveys have been carried out. Recent large-scale structure analyses include (see Strauss & Willick 1995 for a more complete list): (1) nearly all sky samples of objects selected from the *IRAS* Point Source Catalog, specifically the *IRAS* 1.2 Jy survey (5321 galaxies with 60 μm flux $f_{60} > 1.2$ Jy; Fisher et al. 1995) and the 1-in-6 sparse-sampled *IRAS* QDOT Survey (2184 galaxies with $f_{60} > 0.6$ Jy; Lawrence et al. 1996); (2) the Stromlo-APM Survey, selected from the optical APM galaxy catalog, covering 4300 deg^2 of the southern sky to a median survey depth $cz = 15{,}000$ km s^{-1}, but 1-in-20 sparse-sampled (1787 galaxies, $b_J \leq 17.15$; Loveday et al. 1992, 1995; Loveday 1996); and (3) the combined CfA2 and SSRS2 surveys, selected from the Zwicky catalog and from plate scans, respectively, covering one-third of the sky over the north and south Galactic caps out to a mean depth of about 7500 km s^{-1} (14,383 galaxies with $m_{B(0)} \leq 15.5$; Huchra et al. 1996; da Costa et al. 1994a, 1994b). The CfA2 + SSRS2 sample represents the state of the art for a wide-angle survey, with a large sample size and dense sky coverage. Sparse sampling provides an efficient way to measure a particular statistic, while dense sampling reveals structures that require the coherent arrangement of many galaxies and which are not easily characterized by low-order statistics. Our survey has some of the desirable properties of each: the samples are strips on the sky 1°.5 wide and 80° long which are separated by 3°. Within each strip, the galaxies are sampled randomly from a magnitude-limited catalog, but the sampling is quite dense, averaging about 70% of the magnitude-limited list.

TABLE 1

LCRS SAMPLE INFORMATION

Sample	N_{sel}[a]	N_{lsb}[a]	Percentage	N_{gal}[b]	Percentage	N_{star}[b]	Percentage	N[b]	Percentage	f[c]
North 50.....	4288	1179	22	2711	92.2	130	4.4	99	3.4	0.66
South 50	4363	1145	21	2055	91.1	126	5.6	74	3.3	0.50
All 50.....	8651	2324	21	4766	91.7	256	4.9	173	3.3	0.58
North 112.....	12220	557	4	8552	94.9	153	1.7	302	3.4	0.71
South 112.....	15639	1530	9	10379	91.4	451	4.0	525	4.6	0.69
All 112	27859	2087	7	18931	93.0	604	3.0	827	4.1	0.70

[a] N_{sel} is the number of objects which lie within the photometric limits and geometric borders of the sample. N_{lsb} is the number of objects which were excluded because of low central surface brightness (lsb) but were otherwise within the isophotal magnitude limits. The percentage denotes the proportion of lsb objects among all objects within the isophotal magnitude limits.

[b] N_{gal}, N_{star}, and N denote the number of galaxy, stellar, and unidentified spectra, respectively, which were obtained for those objects that met the photometric and boundary limits of the sample. The percentages refer to the proportions of each of the three types among the spectra which were obtained.

[c] f is the galaxy sampling fraction for each sample, corrected for stellar contamination. f is estimated by $f = (N_{gal} + N_{star})/N_{sel}$. We thus assume that the proportion of galaxies and stars among objects with identified spectra is the same as that among objects which were not observed or whose spectra failed to yield an identification.

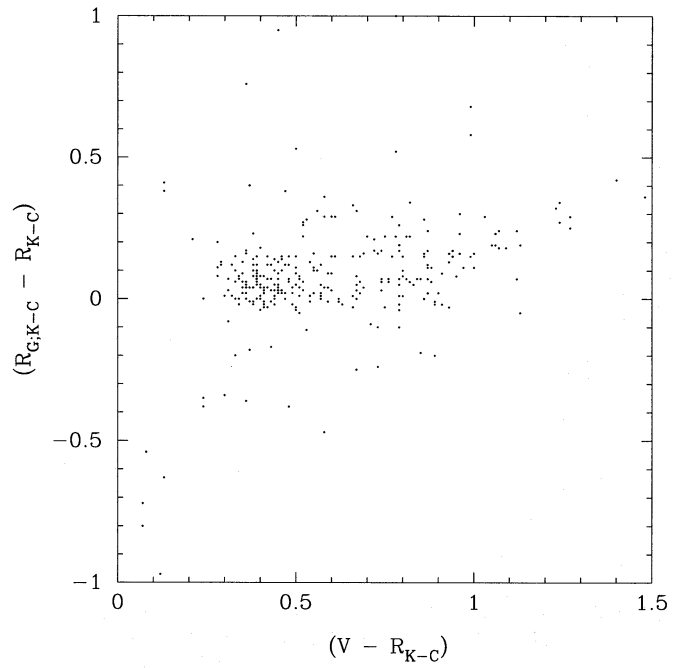

FIG. 2.—Difference between the LCRS hybrid Kron-Cousins R, $R_{G;K-C}$, and true Kron-Cousins R, R_{K-C}, vs. $(V - R_{K-C})$ color. Note that the systematic difference between the two R bands is less than 0.1 mag. (True Kron-Cousins R magnitudes for LCRS objects were obtained from calibration frames taken at the CTIO 0.9 meter telescope.)

The distinctive properties of our survey are its depth (out to 60,000 km s^{-1}) and the number of redshifts (26,000).

The LCRS provides improvements in sample size, volume, and depth in a limited region of the sky. Unlike most previously completed surveys, where spectra were taken of individual galaxies, one at a time, the LCRS employs a fiber-optic spectrograph system on the Las Campanas 2.5 m du Pont telescope to observe over 100 objects at once. The greater depths explored by the LCRS mean that we observe galaxies which have sufficient surface density on the sky to make efficient use of a multifiber system. Some details of the galaxy selection and observing procedure which add to the complexity of the analysis were shaped by the properties of the fiber system, but the overall gain for exploring large-scale structure is very large. In this sense, the LCRS represents part of a fundamental technological change in the way that large-scale redshift surveys are carried out.

Other surveys in progress, such as the Century Survey (Geller et al. 1996) and the ESO-based survey (Vettolani et al. 1993), have a comparable depth but cover smaller areas. Each has selection criteria that differ from ours in interesting ways which should make the comparison of our results with theirs a fruitful enterprise. The next generation of surveys, such as the 2 Degree Field Project (Ellis 1993) and the Sloan Digital Sky Survey (Gunn & Weinberg 1995), will use the multiplex advantage of fiber-fed spectrographs to obtain redshifts of up to a million galaxies, to about the same depth ($z \approx 0.1$) explored by the LCRS. It is our hope to illuminate some of the most interesting subjects for more thorough investigation by these ambitious projects.

In addition to providing a map of the galaxy distribution on the largest scales, the LCRS can help to constrain the physical history of the universe and the properties of its constituents. Current theories of structure formation start with a spectrum of fluctuations produced in the early universe, follow the growth of structure due to gravitation, and

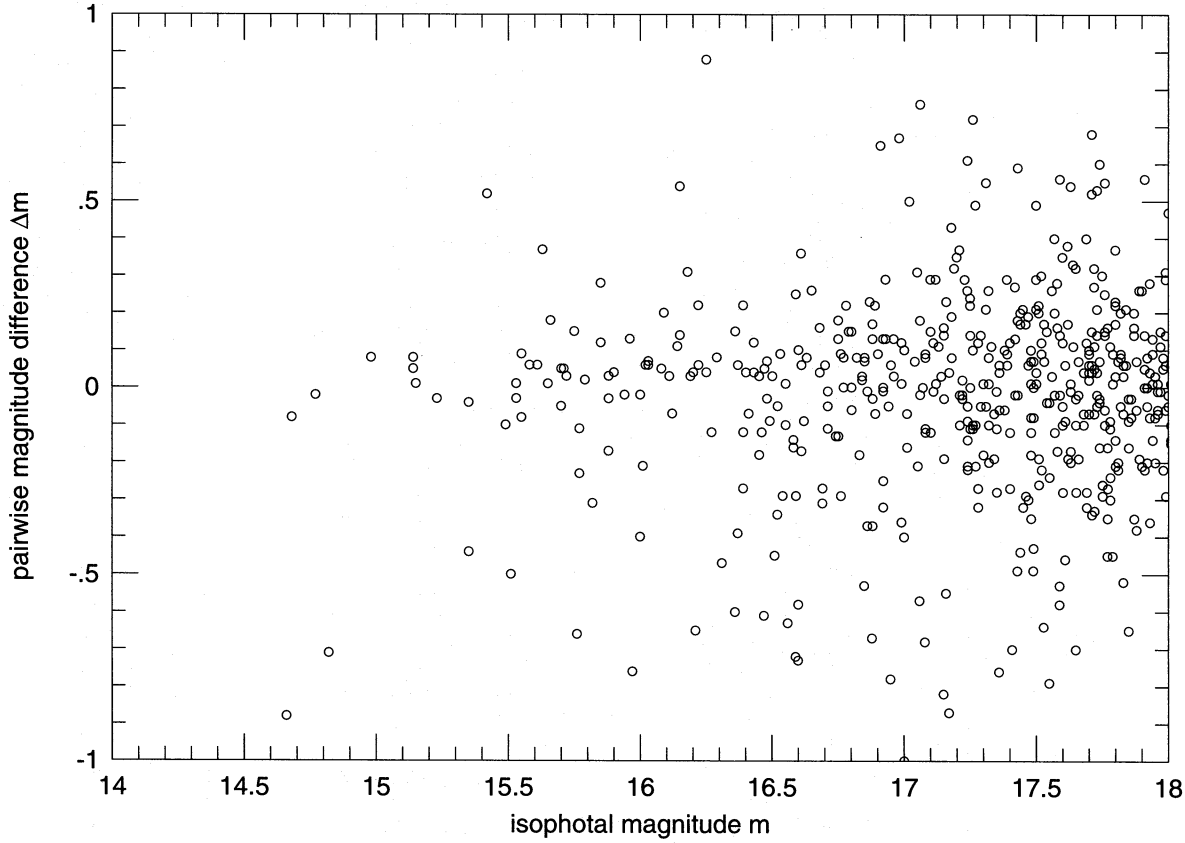

FIG. 3.—Final distribution of pairwise galaxy magnitude differences for galaxies which were measured twice on overlapping bricks of the LCRS

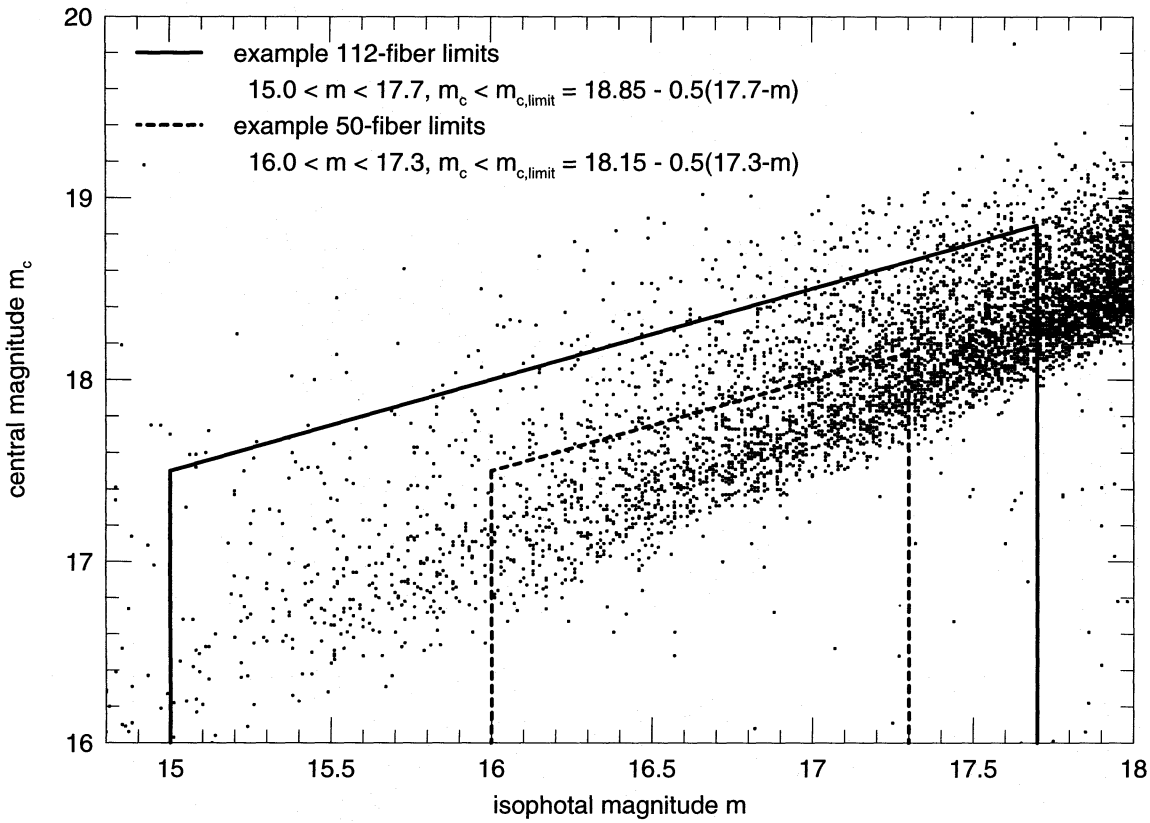

FIG. 4.—Examples of the photometric selection criteria in the isophotal magnitude (m) central magnitude (m_c) plane applied to the 112 and 50 fiber LCRS data.

strive to match both the subtle structure observed at recombination and the high-contrast distribution of the galaxies today mapped by redshift data. Most models presume that the universe is dominated by nonbaryonic dark matter (Blumenthal et al. 1984) the properties of which are to be inferred from the match to the data. The luminous galaxies trace the underlying mass but may be biased: galaxies may form preferentially in peaks of the matter distribution (Bardeen et al. 1986; White et al. 1987). Such models, with the aid of numerical N-body simulations, predict the clustering properties of galaxies from small nonlinear scales of less than 10 h^{-1} Mpc, all the way up past the largest scales sampled by existing redshift surveys. The scales sampled with the LCRS, up to about 300 h^{-1} Mpc, correspond to the horizon size at interesting stages in the early universe and are closer to the scales probed by microwave background observations than can be measured by smaller surveys. By observing galaxy fluctuations on these scales with LCRS, we can learn about primordial density fluctuations and the processes by which they grow. Combining evidence from large-scale structures and from microwave background observations holds the potential to answer fundamental questions about the dark matter that makes up most of the universe (Scott, Silk, & White 1995).

This paper gives details about the construction of the LCRS which are essential to any analysis of the survey data. Some preliminary results and descriptions of the survey have already been published (Shectman et al. 1992, 1995; Oemler et al. 1993; Kirshner 1994; Lin 1995a; Tucker et al. 1995). Tucker (1994) discusses the construction of the survey's photometric catalog and statistical analyses of the early 50 fiber sample. Tucker describes the galaxy correlation function, the properties of galaxy groups, and galaxy clustering as a function of galaxy color. A more complete analysis, using the entire LCRS data set to investigate these topics, will be carried out by Tucker et al. (1996c, 1996a, 1996b, respectively). Lin (1995b) is the basis for the present paper and for several forthcoming papers on the LCRS. Lin et al. (1996a) details the derivation of the luminosity function and space density of LCRS galaxies. Lin et al. (1996b) deals with the power spectrum, a basic statistic which characterizes the clustering properties of galaxies. Lin et al. (1996c) examines redshift-space distortions in the clustering of LCRS galaxies, derives the velocity dispersion of galaxy pairs, and estimates the value of the cosmological density parameter Ω. The analysis of Landy et al. (1996) uses the tools of two-dimensional Fourier analysis to search for coherent structures on very large scales in the LCRS data. Doroshkevich et al. (1996) examine the typical scales and types of large-scale structure in the LCRS sample. Our intention is to make results from this survey and the actual survey data available to interested investigators. We have established a home page for the LCRS at ⟨http://manaslu.astro.utoronto.ca/~lin/lcrs.html⟩ which will provide rapid access to the data. An archival table of the redshift data will accompany this paper as an AAS CD-ROM.

2. SURVEY CONSTRUCTION

The LCRS has been carried out at the Carnegie Institution's Las Campanas Observatory in Chile, with redshifts harvested in a series of 13 spectroscopic observing runs from 1988 November through 1994 October. Over 26,000

galaxy spectra have been gathered, with an average redshift $z = 0.1$, over 700 deg^2 of the sky. This survey has exploited the Las Campanas 2.5 m du Pont telescope's 2°.1 diameter field and the multiplexing capability of the associated multi-object fiber-optic spectrograph system constructed by Shectman, which permits simultaneous observations of 112 galaxy spectra.

The survey data may be divided into two parts based on the development of the photometric detectors and the fiber system during the 6 yr span of the LCRS. The first 20% of the survey galaxies were selected based on data from an 800 × 800 TI CCD, and the redshifts were measured using a 50 object fiber system. Beginning 1991 October, an improved 112 object system was used to gather the final 80% of the data, which were also selected with better imaging systems using first a LORAL, then a large Tektronix CCD. See Table 1 for a summary. Some significant technical details of the survey construction, and additional specifics of the instruments and methods may be found in Shectman et al. (1992, 1995) and Tucker (1994), but essential features which affect the use of the sample for further analysis are set out here.

2.1. *Photometry, Astrometry, and Object Selection*

There was no suitable galaxy catalog available to us in 1986 when preparations for the LCRS began in earnest. We constructed our own catalog through a modest digital sky survey at the 1 m Swope Telescope at Las Campanas. Photometry for the survey comes from CCD drift scans, taken through a Thuan-Gunn r filter (Thuan & Gunn 1976) with the telescope's sidereal drive turned off. The accumulated charge is shifted across the chip at the sidereal rate and read out to produce a continuous strip of photometric data. Three CCD's have been used in this way since the beginning of the survey. The first was a thinned 800 × 800 TI device, which was used with reimaging optics to obtain 1".06 pixels. This was replaced in 1990 with a thick 2K × 2K LORAL chip, used without reimaging optics and binned 2 × 2 to provide 0".865 pixels. The third CCD, introduced in 1992, is a thick 2K × 2K Tektronix CCD used unbinned without reimaging to provide 0".692 pixels. Star-galaxy separation is appreciably better with the latter two chips because of the increased scale and the absence of distortion from intermediate optics.

The effective exposure time depends on the size of the chip and the cosine of the declination, but was typically near 1 minute. The limiting magnitude for the scans is similar to the limiting magnitude of the ESO red plates of the SSRS2 and extended well below the adopted limits near $m = 17.75$ used for galaxy selection. Overlapping scans, offset in declination by slightly less than a chip width, were obtained to build up a strip 1°.5 wide. The typical length of each scan was 3° or 4°.5 long: short enough to complete each 1°.5 × 3° "brick" in about 2 hr, but long enough to minimize the time lost in setting the telescope and initiating the scan. Each brick covers two or three 1°.5 × 1°.5 spectroscopic fields for the fiber system described below. A set of bricks was accumulated over several observing seasons to pave 700 deg^2, arranged in six long paths: in the north Galactic hemisphere at $\delta = -3°$, $-6°$, $-12°$, and in the south Galactic hemisphere at $\delta = -39°$, $-42°$, and $-45°$.

These drift scans were analyzed by an automated photometry system similar to that described in Kirshner et al. (1983). Bias was determined from an overscan region and subtracted from the data. The data were then sky subtracted and flat-fielded using the mode of the pixel values in each column and in each scan-line, respectively. Objects were found by a search routine which identified contiguous groups of pixels whose brightness was greater than 1.15 times that of the sky. Two magnitudes were derived for each object: an isophotal magnitude, m, corresponding to the sum of the background corrected flux in all pixels within the object, and a central magnitude, m_c, which measures the flux within a 2 pixel radius of the object center. The area measured by the central magnitude is close to that covered by a spectroscopic fiber, and it is used to identify galaxies which have low central surface brightness. Images were classified using several structural parameters. All objects not classified as stars were inspected by eye to eliminate spurious galaxy classifications. Our star-galaxy separation criteria turned out to be conservative so that there is a small amount of stellar contamination in the spectroscopic sample (Table 1 and § 2.2). Figure 1 illustrates the stellar contamination rate as a function of isophotal magnitude and surface brightness.

Photometric calibration of the data proceeded in several steps. Observations were obtained only on nights which appeared to be photometric, and photometric standard fields were observed several times per night. These standards were used to obtain a zero point for each night's scans. Though our photometry was obtained with a Gunn r filter, the calibration was done relative to standards

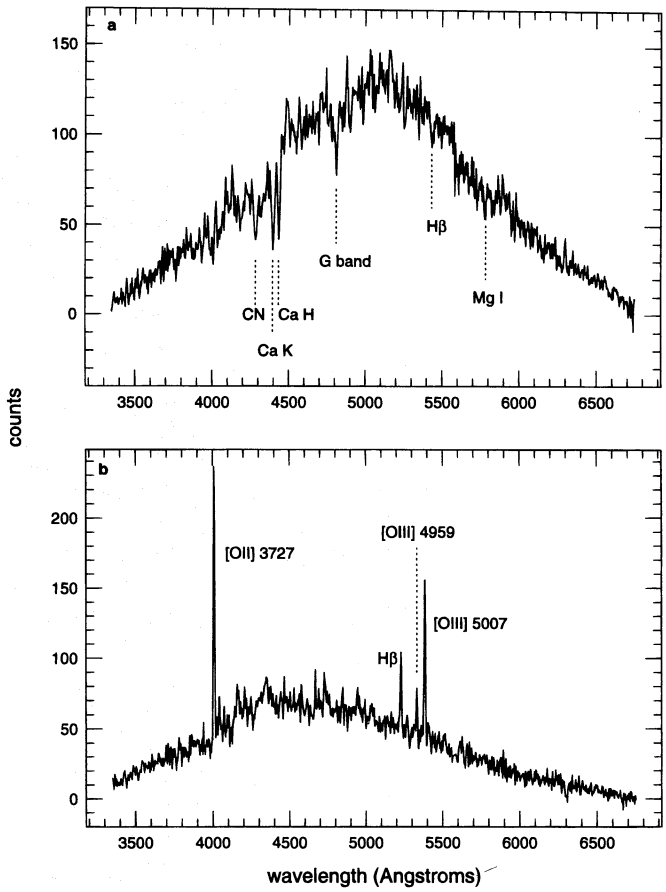

FIG. 5.—Two examples of LCRS galaxy spectra. (*a*) A galaxy with prominent absorption features. (*b*) A galaxy showing strong emission lines.

TABLE 2

LCRS SPECTROSCOPIC FIELDS

Field	α_1[a]	α_2[a]	δ_1[a]	δ_2[a]	m_1[b]	m_2[b]	m_{cen}[b]	N_{fib}[c]	N_{gal}[d]	f[e]
1003-03W.....	10 03 30.60	10 09 46.42	−03 42 28.1	−02 16 03.4	15.06	17.76	19.41	112	111	0.87
1003-03E	10 09 46.42	10 16 05.81	−03 42 28.1	−02 16 03.4	15.06	17.76	19.41	112	109	0.75
1015-03W.....	10 16 05.81	10 21 46.37	−03 44 11.8	−02 15 11.2	14.86	17.56	18.71	112	93	0.56
1015-03E	10 21 46.37	10 28 00.72	−03 44 11.8	−02 15 11.2	14.86	17.56	18.71	112	109	0.57
1027-03W.....	10 28 00.72	10 33 26.78	−03 44 10.7	−02 15 22.0	16.01	17.31	18.31	50	42	0.58
1027-03E	10 33 26.78	10 39 33.77	−03 44 10.7	−02 15 22.0	14.91	17.61	18.76	112	106	0.65
1039-03W.....	10 39 33.77	10 45 30.41	−03 44 16.8	−02 15 14.4	14.94	17.64	18.79	112	97	0.67
1039-03E	10 45 30.41	10 52 00.53	−03 44 16.8	−02 15 14.4	14.94	17.64	18.79	112	101	0.79
1051-03W.....	10 52 00.53	10 57 34.87	−03 44 11.8	−02 15 09.4	16.09	17.39	18.29	50	32	0.89
1051-03E	10 57 34.87	11 03 00.26	−03 44 11.8	−02 15 09.4	16.09	17.39	18.29	50	33	0.94
1103-03W.....	11 03 00.26	11 09 30.94	−03 43 53.0	−02 14 52.4	14.94	17.64	18.79	112	105	0.55
1103-03E	11 09 30.94	11 16 00.74	−03 43 53.0	−02 14 52.4	14.94	17.64	18.79	112	109	0.54
1115-03W.....	11 16 00.74	11 21 29.57	−03 44 03.5	−02 15 02.2	14.73	17.53	18.63	112	95	0.83
1115-03E	11 21 29.57	11 27 00.17	−03 44 03.5	−02 15 02.2	14.73	17.53	18.63	112	67	0.85
1127-03W.....	11 27 00.17	11 33 28.37	−03 44 10.7	−02 14 55.7	14.88	17.58	18.73	112	109	0.71
1127-03E	11 33 28.37	11 39 58.06	−03 44 10.7	−02 14 55.7	14.88	17.58	18.73	112	105	0.52
1139-03W.....	11 39 58.06	11 45 26.45	−03 44 10.3	−02 15 05.8	14.81	17.61	18.71	112	97	0.57
1139-03E	11 45 26.45	11 51 31.18	−03 44 10.3	−02 15 05.8	14.81	17.61	18.71	112	110	0.43
1151-03W.....	11 51 31.18	11 57 30.24	−03 44 33.7	−02 15 08.6	15.01	17.71	18.86	112	88	0.86
1151-03E	11 57 30.24	12 03 42.31	−03 44 33.7	−02 15 08.6	15.01	17.71	18.86	112	95	0.90
1203-03W.....	12 03 42.31	12 09 31.32	−03 44 41.3	−02 15 16.2	15.05	17.65	18.85	112	96	0.89
1203-03E	12 09 31.32	12 15 31.30	−03 44 41.3	−02 15 16.2	15.05	17.65	18.85	112	108	0.59
1215-03W.....	12 15 31.30	12 21 28.97	−03 44 12.5	−02 15 09.7	14.79	17.59	18.69	112	104	0.86
1215-03E	12 21 28.97	12 27 29.74	−03 44 12.5	−02 15 09.7	14.79	17.59	18.69	112	104	0.89
1227-03W.....	12 27 29.74	12 33 27.70	−03 46 05.2	−02 15 20.9	15.92	17.22	18.07	50	33	0.82
1227-03E	12 33 27.70	12 39 18.65	−03 46 05.2	−02 15 20.9	15.92	17.22	18.07	50	48	0.91
1239-03W.....	12 39 28.66	12 45 27.94	−03 43 28.9	−02 15 25.9	15.85	17.15	18.00	50	25	0.45
1239-03E	12 45 27.94	12 51 19.46	−03 43 28.9	−02 15 25.9	15.85	17.15	18.00	50	43	0.76
1251-03W.....	12 51 23.11	12 57 21.41	−03 46 22.4	−02 15 34.9	15.83	17.13	18.08	50	47	0.63
1251-03E	12 57 21.41	13 03 13.54	−03 46 22.4	−02 15 34.9	15.83	17.13	18.08	50	47	0.37
1303-03W.....	13 03 30.26	13 09 25.20	−03 46 21.0	−02 15 19.4	16.00	17.30	18.15	50	45	0.68
1303-03E	13 09 25.20	13 15 19.58	−03 46 21.0	−02 15 19.4	16.00	17.30	18.15	50	39	0.89
1315-03W.....	13 15 26.62	13 21 20.71	−03 45 55.1	−02 15 04.3	15.88	17.18	18.13	50	49	0.67
1315-03E	13 21 20.71	13 27 13.63	−03 45 55.1	−02 15 04.3	15.88	17.18	18.13	50	50	0.53
1327-03W.....	13 27 28.51	13 33 24.96	−03 44 44.2	−02 15 39.2	16.03	17.33	18.33	50	50	0.59
1327-03E	13 33 24.96	13 39 29.93	−03 44 44.2	−02 15 39.2	14.93	17.63	18.78	112	107	0.81
1339-03W.....	13 39 30.62	13 45 30.00	−03 44 20.4	−02 15 33.8	14.81	17.61	18.71	112	78	0.72
1339-03E	13 45 30.00	13 50 59.86	−03 44 20.4	−02 15 33.8	14.81	17.61	18.71	112	80	0.89
1351-03W.....	13 50 59.86	13 57 31.73	−03 44 24.7	−02 15 29.9	14.77	17.47	18.62	112	104	0.93
1351-03E	13 57 31.73	14 04 00.00	−03 44 24.7	−02 15 29.9	14.77	17.47	18.62	112	96	0.86
1403-03W.....	14 04 00.00	14 09 30.10	−03 44 11.4	−02 15 21.2	14.78	17.58	18.68	112	94	0.85
1403-03E	14 09 30.10	14 14 59.52	−03 44 11.4	−02 15 21.2	14.78	17.58	18.68	112	89	0.92
1415-03W.....	14 14 59.52	14 21 24.12	−03 44 21.1	−02 15 18.7	15.01	17.71	18.86	112	103	0.91
1415-03E	14 21 24.12	14 27 57.67	−03 44 21.1	−02 15 18.7	15.01	17.71	18.86	112	108	0.91
1427-03W.....	14 27 57.67	14 33 31.15	−03 44 47.8	−02 15 49.3	16.14	17.44	18.44	50	26	0.83
1427-03E	14 33 31.15	14 39 00.34	−03 44 47.8	−02 15 49.3	16.14	17.44	18.44	50	41	0.88
1439-03W.....	14 39 00.34	14 45 25.46	−03 44 17.5	−02 15 14.0	15.11	17.81	18.96	112	107	0.72
1439-03E	14 45 25.46	14 51 57.19	−03 44 17.5	−02 15 14.0	15.11	17.81	18.96	112	108	0.91
1451-03W.....	14 51 57.19	14 57 11.54	−03 46 22.8	−02 15 37.1	15.96	17.26	18.11	50	37	0.70
1451-03E	14 57 11.54	15 03 02.04	−03 46 22.8	−02 15 37.1	15.96	17.26	18.11	50	25	0.97
1503-03W.....	15 03 02.04	15 09 30.22	−03 44 12.1	−02 15 14.0	14.76	17.56	18.66	112	63	0.92
1503-03E	15 09 30.22	15 15 30.17	−03 44 12.1	−02 15 14.0	14.76	17.56	18.66	112	100	0.72
1515-03W.....	15 15 30.17	15 21 30.82	−03 44 38.0	−02 15 43.6	14.89	17.69	18.79	112	66	0.91
1515-03E	15 21 30.82	15 27 30.02	−03 44 38.0	−02 15 43.6	14.89	17.69	18.74	112	62	0.91
1003-06W.....	10 03 30.96	10 09 52.32	−06 42 12.6	−05 15 49.0	15.00	17.70	19.35	112	100	0.55
1003-06E	10 09 52.32	10 16 08.62	−06 42 12.6	−05 15 49.0	15.00	17.70	19.35	112	92	0.88
1015-06W.....	10 16 08.62	10 21 17.71	−06 43 56.3	−05 15 33.8	15.98	17.28	18.13	50	38	0.39
1015-06E	10 21 17.71	10 27 06.96	−06 43 56.3	−05 15 33.8	15.98	17.28	18.13	50	44	0.81
1027-06W.....	10 27 30.82	10 33 33.17	−06 44 26.9	−05 15 13.3	15.92	17.22	18.22	50	45	0.66
1027-06E	10 33 33.17	10 39 37.18	−06 44 26.9	−05 15 13.3	15.92	17.22	18.22	50	38	0.76
1039-06W.....	10 39 37.18	10 45 02.45	−06 43 53.4	−05 15 25.2	16.26	17.56	18.41	50	44	0.90
1039-06E	10 45 02.45	10 51 06.14	−06 43 53.4	−05 15 25.2	16.26	17.56	18.41	50	46	0.48
1051-06W.....	10 51 31.66	10 57 11.11	−06 44 15.0	−05 15 23.0	16.08	17.38	18.28	50	48	0.60
1051-06E	10 57 11.11	11 03 27.31	−06 44 15.0	−05 15 23.0	16.08	17.38	18.28	50	48	0.66
1103-06W.....	11 03 28.44	11 09 18.22	−06 44 19.0	−05 15 27.4	16.03	17.33	18.28	50	40	0.93
1103-06E	11 09 18.22	11 15 05.64	−06 44 19.0	−05 15 27.4	16.03	17.33	18.28	50	39	0.51
1115-06W.....	11 15 30.91	11 21 28.03	−06 44 31.6	−05 15 26.3	16.08	17.38	18.38	50	48	0.83
1115-06E	11 21 28.03	11 27 38.09	−06 44 31.6	−05 15 26.3	16.08	17.38	18.38	50	50	0.85
1127-06W.....	11 27 38.09	11 33 11.81	−06 31 41.2	−05 15 32.0	16.01	17.31	18.16	50	48	0.69
1127-06E	11 33 11.81	11 39 05.69	−06 31 41.2	−05 15 32.0	16.01	17.31	18.16	50	36	0.93
1139-06W.....	11 39 28.82	11 45 30.91	−06 44 22.9	−05 15 01.1	14.98	17.68	18.83	112	109	0.74
1139-06E	11 45 30.91	11 51 34.61	−06 44 22.9	−05 15 01.1	16.08	17.38	18.38	50	47	0.52
1151-06W.....	11 51 34.61	11 57 09.77	−06 44 21.1	−05 15 27.0	16.04	17.34	18.19	50	45	0.65
1151-06E	11 57 09.77	12 03 07.08	−06 44 21.1	−05 15 27.0	16.04	17.34	18.19	50	46	0.58

TABLE 2—*Continued*

Field	α_1[a]	α_2[a]	δ_1[a]	δ_2[a]	m_1[b]	m_2[b]	m_{cen}[b]	N_{fib}[c]	N_{gal}[d]	f[e]
1203-06W.....	12 03 30.98	12 09 36.02	−06 44 44.9	−05 15 18.7	16.02	17.32	18.22	50	46	0.63
1203-06E	12 09 36.02	12 15 36.74	−06 44 44.9	−05 15 18.7	16.02	17.32	18.22	50	46	0.42
1215-06W.....	12 15 36.74	12 21 16.92	−06 44 15.7	−05 15 38.9	16.07	17.37	18.22	50	41	0.92
1215-06E	12 21 16.92	12 27 07.68	−06 44 15.7	−05 15 38.9	16.07	17.37	18.22	50	37	0.93
1227-06W.....	12 27 30.17	12 33 27.58	−06 44 22.9	−05 15 23.8	16.16	17.46	18.36	50	38	0.76
1227-06E	12 33 27.58	12 39 36.74	−06 44 22.9	−05 15 23.8	16.16	17.46	18.36	50	48	0.68
1239-06W.....	12 39 36.74	12 45 11.78	−06 44 15.4	−05 15 28.4	16.13	17.43	18.28	50	43	0.47
1239-06E	12 45 11.78	12 51 06.84	−06 44 15.4	−05 15 28.4	16.13	17.43	18.28	50	43	0.47
1251-06W.....	12 51 29.11	12 57 28.78	−06 44 39.1	−05 15 12.2	16.10	17.40	18.40	50	46	0.76
1251-06E	12 57 28.78	13 03 33.10	−06 44 39.1	−05 15 12.2	16.10	17.40	18.40	50	47	0.53
1303-06W.....	13 03 33.10	13 09 22.85	−06 44 19.0	−05 15 36.7	16.28	17.58	18.43	50	44	0.51
1303-06E	13 09 22.85	13 15 05.14	−06 44 19.0	−05 15 36.7	16.28	17.58	18.43	50	39	0.51
1315-06W.....	13 15 28.56	13 21 38.35	−06 44 37.7	−05 15 29.5	15.00	17.70	18.85	112	68	0.71
1315-06E	13 21 38.35	13 27 29.02	−06 44 37.7	−05 15 29.5	16.10	17.40	18.30	50	28	0.84
1327-06W.....	13 27 29.02	13 33 17.66	−06 44 25.4	−05 15 50.4	15.98	17.28	18.13	50	50	0.93
1327-06E	13 33 17.66	13 39 07.70	−06 44 25.4	−05 15 50.4	15.98	17.28	18.13	50	48	0.59
1339-06W.....	13 39 31.06	13 45 34.39	−06 31 58.4	−05 15 06.1	16.03	17.33	18.23	50	47	0.70
1339-06E	13 45 34.39	13 51 35.93	−06 31 58.4	−05 15 06.1	16.03	17.33	18.23	50	40	0.89
1351-06W.....	13 51 35.93	13 57 15.53	−06 44 16.8	−05 15 37.4	15.83	17.13	17.98	50	31	0.92
1351-06E	13 57 15.53	14 03 04.18	−06 44 16.8	−05 15 37.4	15.83	17.13	17.98	50	49	0.72
1403-06W.....	14 03 31.75	14 09 34.92	−06 44 52.4	−05 15 46.8	16.07	17.37	18.37	50	43	0.64
1403-06E	14 09 34.92	14 15 36.55	−06 44 52.4	−05 15 46.8	16.07	17.37	18.37	50	48	0.83
1415-06W.....	14 15 36.55	14 21 07.15	−06 19 08.8	−05 15 51.5	16.06	17.36	18.21	50	36	0.82
1415-06E	14 21 07.15	14 27 06.41	−06 19 08.8	−05 15 51.5	16.06	17.36	18.21	50	17	0.86
1427-06W.....	14 27 28.70	14 33 45.29	−06 44 51.4	−05 40 55.2	16.10	17.40	18.30	50	26	0.86
1427-06E	14 33 45.29	14 39 35.18	−06 44 51.4	−05 40 55.2	16.10	17.40	18.30	50	26	0.76
1439-06W.....	14 39 35.18	14 45 18.74	−06 44 25.8	−05 15 51.1	16.18	17.48	18.33	50	45	0.66
1439-06E	14 45 18.74	14 51 06.48	−06 44 25.8	−05 15 51.1	16.18	17.48	18.33	50	42	0.62
1451-06W.....	14 51 29.76	14 57 34.42	−06 44 50.6	−05 15 35.6	16.13	17.43	18.43	50	30	0.66
1451-06E	14 57 34.42	15 03 28.32	−06 44 50.6	−05 15 35.6	16.13	17.43	18.43	50	33	0.75
1503-06W.....	15 03 28.32	15 09 19.63	−06 44 28.7	−05 15 45.4	16.04	17.34	18.29	50	44	0.61
1503-06E	15 09 19.63	15 15 00.38	−06 44 28.7	−05 15 45.4	16.04	17.34	18.29	50	47	0.77
1003-12W.....	10 03 26.02	10 09 50.81	−12 42 16.6	−11 15 49.7	14.91	17.61	19.26	112	79	0.87
1003-12E	10 09 50.81	10 15 00.58	−12 42 16.6	−11 15 49.7	14.91	17.61	19.26	112	64	0.85
1015-12W.....	10 15 00.58	10 21 30.48	−12 42 59.8	−11 16 29.6	15.02	17.72	19.27	112	97	0.80
1015-12E	10 21 30.48	10 27 00.53	−12 42 59.8	−11 16 29.6	15.02	17.72	19.27	112	102	0.85
1027-12W.....	10 27 00.53	10 33 38.28	−12 43 58.8	−11 15 01.4	15.01	17.71	18.86	112	107	0.77
1027-12E	10 33 38.28	10 39 00.22	−12 43 58.8	−11 15 01.4	15.01	17.71	18.86	112	87	0.67
1039-12W.....	10 39 00.22	10 45 28.01	−12 42 41.0	−11 16 11.6	15.03	17.73	19.28	112	103	0.68
1039-12E	10 45 28.01	10 51 59.69	−12 42 41.0	−11 16 11.6	15.03	17.73	19.28	112	111	0.73
1051-12W.....	10 51 59.69	10 57 37.80	−12 42 06.8	−11 15 36.7	15.08	17.78	19.43	112	93	0.49
1051-12E	10 57 37.80	11 04 16.75	−12 42 06.8	−11 15 36.7	15.08	17.78	19.43	112	105	0.79
1103-12W.....	11 04 16.75	11 09 30.36	−12 43 00.8	−11 16 36.5	15.03	17.73	19.28	112	69	0.89
1103-12E	11 09 30.36	11 15 58.27	−12 43 00.8	−11 16 36.5	15.03	17.73	19.28	112	109	0.59
1115-12W.....	11 15 58.27	11 21 35.30	−12 42 11.5	−11 16 03.0	15.01	17.71	19.36	112	90	0.82
1115-12E	11 21 35.30	11 28 18.50	−12 42 11.5	−11 16 03.0	15.01	17.71	19.36	112	109	0.81
1127-12W.....	11 28 18.50	11 33 37.63	−12 43 14.2	−11 16 28.6	15.01	17.71	19.26	112	99	0.51
1127-12E	11 33 37.63	11 39 01.63	−12 43 14.2	−11 16 28.6	15.01	17.71	19.26	112	102	0.45
1139-12W.....	11 39 01.63	11 45 41.33	−12 43 01.6	−11 16 20.3	15.00	17.70	19.35	112	110	0.54
1139-12E	11 45 41.33	11 52 20.90	−12 43 01.6	−11 16 20.3	15.00	17.70	19.35	112	109	0.68
1151-12W.....	11 52 20.90	11 57 29.23	−12 42 58.7	−11 16 17.8	15.03	17.73	19.28	112	90	0.79
1151-12E	11 57 29.23	12 03 00.91	−12 42 58.7	−11 16 17.8	15.03	17.73	19.28	112	54	0.77
1203-12W.....	12 03 00.91	12 09 39.19	−12 42 55.8	−11 16 20.6	15.03	17.73	19.38	112	75	0.89
1203-12E	12 09 39.19	12 15 00.48	−12 42 55.8	−11 16 20.6	15.03	17.73	19.38	112	84	0.86
1215-12W.....	12 15 00.48	12 21 27.07	−12 43 14.2	−11 16 34.3	15.04	17.74	19.29	112	82	0.79
1215-12E	12 21 27.07	12 26 58.68	−12 43 14.2	−11 16 34.3	15.04	17.74	19.29	112	72	0.87
1227-12W.....	12 26 58.68	12 33 37.20	−12 42 40.3	−11 37 09.1	15.10	17.80	19.45	112	105	0.87
1227-12E	12 33 37.20	12 40 19.08	−12 42 40.3	−11 37 09.1	15.10	17.80	19.45	112	99	0.89
1239-12W.....	12 40 19.08	12 45 32.21	−12 43 21.7	−11 16 50.5	14.92	17.62	19.17	112	83	0.57
1239-12E	12 45 32.21	12 51 58.68	−12 43 21.7	−11 16 50.5	14.92	17.62	19.17	112	110	0.63
1251-12W.....	12 51 58.68	12 57 38.47	−12 42 49.7	−11 16 21.7	15.03	17.73	19.38	112	93	0.47
1251-12E	12 57 38.47	13 04 18.02	−12 42 49.7	−11 16 21.7	15.03	17.73	19.38	112	106	0.91
1303-12W.....	13 04 18.02	13 09 31.51	−12 43 20.3	−11 16 59.2	14.97	17.67	19.22	112	68	0.87
1303-12E	13 09 31.51	13 15 59.11	−12 43 20.3	−11 16 59.2	14.97	17.67	19.22	112	92	0.86
1315-12W.....	13 15 59.11	13 21 39.19	−12 42 31.7	−11 16 13.8	14.92	17.62	19.27	112	57	0.76
1315-12E	13 21 39.19	13 28 17.59	−12 42 31.7	−11 16 13.8	14.92	17.62	19.27	112	108	0.83
1327-12W.....	13 28 17.59	13 33 30.17	−12 43 05.9	−11 16 42.2	15.05	17.75	19.30	112	96	0.50
1327-12E	13 33 30.17	13 39 58.15	−12 43 05.9	−11 16 42.2	15.05	17.75	19.30	112	108	0.59
1339-12W.....	13 39 58.15	13 45 44.42	−12 42 58.0	−11 16 44.0	14.87	17.57	19.22	112	89	0.81
1339-12E	13 45 44.42	13 52 17.78	−12 42 58.0	−11 16 44.0	14.87	17.57	19.22	112	105	0.51
1351-12W.....	13 52 17.78	13 57 16.34	−12 43 23.5	−11 17 00.2	14.95	17.65	19.20	112	93	0.57
1351-12E	13 57 16.34	14 04 01.10	−12 43 23.5	−11 17 00.2	14.95	17.65	19.20	112	109	0.76
1403-12W.....	14 04 01.10	14 09 38.64	−12 43 01.2	−11 16 44.4	14.98	17.68	19.33	112	94	0.66

TABLE 2—*Continued*

Field	α_1[a]	α_2[a]	δ_1[a]	δ_2[a]	m_1[b]	m_2[b]	m_{cen}[b]	N_{fib}[c]	N_{gal}[d]	f[e]
1403-12E	14 09 38.64	14 16 16.68	−12 43 01.2	−11 16 44.4	14.98	17.68	19.33	112	78	0.86
1415-12W.....	14 16 16.68	14 20 47.78	−12 43 19.9	−11 17 07.1	14.97	17.77	19.27	112	42	0.93
1415-12E	14 20 47.78	14 27 00.82	−12 43 19.9	−11 17 07.1	14.97	17.77	19.27	112	35	0.90
1427-12W.....	14 27 00.82	14 33 38.88	−12 44 36.2	−11 15 47.2	14.89	17.69	18.79	112	66	0.81
1427-12E	14 33 38.88	14 40 15.60	−12 44 36.2	−11 15 47.2	14.89	17.69	18.79	112	92	0.86
1439-12W.....	14 40 15.60	14 45 30.67	−12 43 17.8	−11 17 12.5	15.02	17.92	19.37	112	70	0.63
1439-12E	14 45 30.67	14 51 57.58	−12 43 17.8	−11 17 12.5	15.02	17.92	19.37	112	103	0.67
1451-12W.....	14 51 57.58	14 57 35.62	−12 44 36.2	−11 15 41.4	14.80	17.60	18.70	112	62	0.86
1451-12E	14 57 35.62	15 04 16.87	−12 44 36.2	−11 15 41.4	14.80	17.60	18.70	112	78	0.83
1503-12W.....	15 04 16.87	15 09 32.42	−12 43 23.5	−11 17 19.0	15.04	17.94	19.39	112	90	0.69
1503-12E	15 09 32.42	15 15 57.79	−12 43 23.5	−11 17 19.0	15.04	17.94	19.39	112	92	0.78
1515-12W.....	15 15 57.79	15 21 24.53	−12 21 13.0	−11 16 40.8	14.92	17.92	19.42	112	44	0.72
1515-12E	15 21 24.53	15 27 50.71	−12 21 13.0	−11 16 40.8	14.92	17.92	19.42	112	47	0.82
2100-39W.....	21 00 40.22	21 07 58.73	−39 46 18.8	−38 16 13.8	16.03	17.33	18.18	50	41	0.30
2100-39E	21 07 58.73	21 15 11.04	−39 46 18.8	−38 16 13.8	15.03	17.54	18.48	112	79	0.54
2114-39W.....	21 15 11.04	21 23 55.27	−39 44 43.1	−38 16 16.7	14.93	17.63	18.78	112	80	0.80
2114-39M.....	21 23 55.27	21 32 36.58	−39 44 43.1	−38 16 16.7	14.93	17.63	18.78	112	89	0.68
2114-39E	21 32 36.58	21 41 11.35	−39 44 43.1	−38 16 16.7	14.93	17.63	18.78	112	97	0.65
2140-39W.....	21 41 11.35	21 48 15.12	−39 44 25.1	−38 15 41.0	15.95	17.25	18.10	50	32	0.75
2140-39E	21 48 15.12	21 55 09.46	−39 44 25.1	−38 15 41.0	15.95	17.25	18.10	50	28	0.83
2154-39W.....	21 55 09.46	22 03 54.89	−39 44 26.9	−38 15 58.7	14.95	17.65	18.80	112	67	0.74
2154-39M.....	22 03 54.89	22 12 40.30	−39 44 26.9	−38 15 58.7	14.95	17.65	18.80	112	88	0.65
2154-39E	22 12 40.30	22 21 11.04	−39 44 26.9	−38 15 58.7	14.95	17.65	18.80	112	108	0.59
2220-39W.....	22 21 11.04	22 28 12.58	−39 44 25.1	−38 15 25.9	16.15	17.45	18.30	50	45	0.62
2220-39E	22 28 12.58	22 35 09.96	−39 44 25.1	−38 15 25.9	16.15	17.45	18.30	50	44	0.35
2234-39W.....	22 35 09.96	22 43 52.30	−39 44 55.7	−38 16 17.0	14.83	17.53	18.68	112	105	0.52
2234-39M.....	22 43 52.30	22 52 46.75	−39 44 55.7	−38 16 17.0	14.83	17.53	18.68	112	103	0.83
2234-39E	22 52 46.75	23 01 11.83	−39 44 55.7	−38 16 17.0	14.83	17.53	18.68	112	100	0.73
2300-39W.....	23 01 11.83	23 08 16.87	−39 44 28.0	−38 15 25.6	16.03	17.33	18.18	50	37	0.64
2300-39E	23 08 16.87	23 15 11.21	−39 44 28.0	−38 15 25.6	16.03	17.33	18.18	50	41	0.58
2314-39W.....	23 15 11.21	23 24 06.12	−39 44 06.4	−38 15 19.4	14.98	17.68	18.83	112	91	0.83
2314-39M.....	23 24 06.12	23 32 38.35	−39 44 06.4	−38 15 19.4	14.98	17.68	18.83	112	106	0.65
2314-39E	23 32 38.35	23 41 13.18	−39 44 06.4	−38 15 19.4	14.98	17.68	18.83	112	99	0.58
2340-39W.....	23 41 13.18	23 48 15.58	−39 44 23.6	−38 15 07.6	16.21	17.51	18.36	50	40	0.41
2340-39E	23 48 15.58	23 55 09.77	−39 44 23.6	−38 15 07.6	16.21	17.51	18.36	50	45	0.41
2354-39W.....	23 55 09.77	00 04 01.22	−39 44 26.5	−38 15 25.9	15.03	17.73	18.98	112	106	0.56
2354-39M.....	00 04 01.22	00 12 35.35	−39 44 26.5	−38 15 25.9	15.03	17.73	18.98	112	105	0.69
2354-39E	00 12 35.35	00 21 12.12	−39 44 26.5	−38 15 25.9	15.03	17.73	18.98	112	105	0.59
0020-39W.....	00 21 12.12	00 28 14.21	−39 44 32.6	−38 28 18.5	16.12	17.42	18.27	50	36	0.46
0020-39E	00 28 14.21	00 35 10.54	−39 44 32.6	−38 28 18.5	16.12	17.42	18.27	50	39	0.35
0034-39W.....	00 35 10.54	00 43 51.72	−39 44 48.5	−38 15 53.3	15.03	17.73	18.88	112	107	0.74
0034-39M.....	00 43 51.72	00 52 42.79	−39 44 48.5	−38 15 53.3	15.03	17.73	18.88	112	97	0.86
0034-39E	00 52 42.79	01 01 13.30	−39 44 48.5	−38 15 53.3	15.03	17.73	18.88	112	93	0.83
0100-39W.....	01 01 13.30	01 08 21.22	−39 44 19.3	−38 15 19.8	16.08	17.38	18.23	50	42	0.64
0100-39E	01 08 21.22	01 15 09.70	−39 44 19.3	−38 15 19.8	16.08	17.38	18.23	50	39	0.45
0114-39W.....	01 15 09.70	01 23 51.65	−39 43 48.4	−38 15 16.2	14.99	17.69	18.94	112	103	0.50
0114-39M.....	01 23 51.65	01 32 27.38	−39 43 48.4	−38 15 16.2	14.99	17.69	18.94	112	97	0.64
0114-39E	01 32 27.38	01 41 11.40	−39 43 48.4	−38 15 16.2	14.99	17.69	18.94	112	89	0.85
0140-39W.....	01 41 11.40	01 48 47.62	−39 44 04.9	−38 15 14.0	16.14	17.44	18.29	50	24	1.00
0140-39E	01 48 47.62	01 55 09.72	−39 44 04.9	−38 15 14.0	16.14	17.44	18.29	50	26	0.63
0154-39W.....	01 55 09.72	02 03 53.90	−39 43 48.4	−38 15 14.8	14.92	17.62	18.77	112	88	0.62
0154-39M.....	02 03 53.90	02 12 43.75	−39 43 48.4	−38 15 14.8	14.92	17.62	18.77	112	75	0.92
0154-39E	02 12 43.75	02 21 02.59	−39 43 48.4	−38 15 14.8	14.92	17.62	18.77	112	86	0.89
0220-39W.....	02 21 02.59	02 28 13.27	−39 44 09.6	−38 15 05.8	16.15	17.45	18.30	50	43	0.88
0220-39E	02 28 13.27	02 35 11.62	−39 44 09.6	−38 15 05.8	16.15	17.45	18.30	50	47	0.83
0234-39W.....	02 35 11.62	02 43 52.44	−39 43 38.6	−38 15 13.3	14.86	17.56	18.71	112	99	0.88
0234-39M.....	02 43 52.44	02 52 49.39	−39 43 38.6	−38 15 13.3	14.86	17.56	18.71	112	78	0.81
0234-39E	02 52 49.39	03 01 10.68	−39 43 38.6	−38 15 13.3	14.86	17.56	18.71	112	101	0.82
0300-39W.....	03 01 10.68	03 08 16.39	−39 44 00.6	−38 15 28.1	16.02	17.32	18.27	50	36	0.31
0300-39E	03 08 16.39	03 15 09.34	−39 44 00.6	−38 15 28.1	16.02	17.32	18.27	50	40	0.39
0314-39W.....	03 15 09.34	03 23 57.19	−39 43 31.8	−38 15 06.1	15.02	17.72	18.87	112	105	0.61
0314-39M.....	03 23 57.19	03 32 42.67	−39 43 31.8	−38 15 06.1	15.02	17.72	18.87	112	108	0.57
0314-39E	03 32 42.67	03 41 10.85	−39 43 31.8	−38 15 06.1	15.02	17.72	18.87	112	107	0.44
0340-39W.....	03 41 10.85	03 48 17.93	−39 44 10.7	−38 15 16.9	16.18	17.48	18.33	50	46	0.62
0340-39E	03 48 17.93	03 55 11.62	−39 44 10.7	−38 15 16.9	16.18	17.48	18.33	50	40	0.46
0354-39W.....	03 55 11.62	04 03 53.64	−39 43 18.1	−38 15 20.5	14.92	17.62	18.77	112	102	0.68
0354-39M.....	04 03 53.64	04 12 47.11	−39 43 18.1	−38 15 20.5	14.92	17.62	18.77	112	82	0.82
0354-39E	04 12 47.11	04 21 11.88	−39 43 18.1	−38 15 20.5	14.92	17.62	18.77	112	95	0.82
0420-39W.....	04 21 11.88	04 28 22.97	−39 44 04.6	−38 15 46.1	16.07	17.37	18.22	50	31	0.49
0420-39E	04 28 22.97	04 35 49.25	−39 44 04.6	−38 15 46.1	16.07	17.37	18.22	50	26	0.69
2100-42W.....	21 03 46.03	21 12 04.30	−42 44 31.9	−41 40 38.3	14.79	17.59	18.69	112	103	0.80
2100-42E	21 12 04.30	21 20 22.70	−42 44 31.9	−41 40 38.3	14.79	17.59	18.69	112	80	0.85
2120-42W.....	21 20 43.92	21 28 49.03	−42 44 55.3	−41 16 05.5	14.89	17.69	18.79	112	84	0.63

TABLE 2—*Continued*

Field	α_1[a]	α_2[a]	δ_1[a]	δ_2[a]	m_1[b]	m_2[b]	m_{cen}[b]	N_{fib}[c]	N_{gal}[d]	f[e]
2120-42E	21 28 49.03	21 35 44.57	−42 44 55.3	−41 16 05.5	14.89	17.69	18.79	112	80	0.52
2135-42W.....	21 35 44.57	21 43 45.19	−42 44 19.3	−41 15 30.2	14.82	17.52	18.82	112	102	0.84
2135-42M.....	21 43 45.19	21 52 50.28	−42 44 19.3	−41 15 30.2	14.82	17.52	18.82	112	84	0.85
2135-42E	21 52 50.28	22 01 22.10	−42 44 19.3	−41 15 30.2	14.82	17.52	18.82	112	77	0.81
2200-42W.....	22 01 22.10	22 08 40.54	−42 45 11.2	−41 16 20.6	14.76	17.56	18.66	112	73	0.91
2200-42E	22 08 40.54	22 15 43.92	−42 45 11.2	−41 16 20.6	14.76	17.56	18.66	112	53	0.78
2215-42W.....	22 15 43.92	22 23 51.84	−42 44 02.4	−41 14 47.0	14.83	17.53	18.83	112	102	0.83
2215-42M.....	22 23 51.84	22 32 57.19	−42 44 02.4	−41 14 47.0	14.83	17.53	18.83	112	106	0.67
2215-42E	22 32 57.19	22 41 22.82	−42 44 02.4	−41 14 47.0	14.83	17.53	18.83	112	106	0.65
2240-42W.....	22 41 22.82	22 48 47.59	−42 45 13.0	−41 16 05.2	14.92	17.72	19.02	112	89	0.68
2240-42E	22 48 47.59	22 56 43.73	−42 45 13.0	−41 16 05.2	14.92	17.72	19.02	112	101	0.92
2255-42W.....	22 56 43.73	23 03 40.49	−42 44 43.4	−41 15 18.4	14.84	17.54	18.59	112	78	0.77
2255-42M.....	23 03 40.49	23 12 57.48	−42 44 43.4	−41 15 18.4	14.84	17.54	18.59	112	101	0.82
2255-42E	23 12 57.48	23 21 19.94	−42 44 43.4	−41 15 18.4	14.84	17.54	18.59	112	106	0.34
2320-42W.....	23 21 19.94	23 28 33.14	−42 44 38.4	−41 15 31.7	16.26	17.56	18.41	50	37	0.58
2320-42E	23 28 33.14	23 35 44.54	−42 44 38.4	−41 15 31.7	16.26	17.56	18.41	50	39	0.95
2335-42W.....	23 35 44.54	23 43 43.99	−42 44 20.8	−41 14 53.2	15.04	17.74	18.99	112	101	0.76
2335-42M.....	23 43 43.99	23 52 56.16	−42 44 20.8	−41 14 53.2	15.04	17.74	18.99	112	99	0.90
2335-42E	23 52 56.16	00 01 25.73	−42 44 20.8	−41 14 53.2	15.04	17.74	18.99	112	103	0.65
0000-42W.....	00 01 25.73	00 08 28.66	−42 44 04.6	−41 15 28.8	16.19	17.49	18.34	50	40	0.35
0000-42E	00 08 28.66	00 15 43.22	−42 44 04.6	−41 15 28.8	16.19	17.49	18.34	50	37	0.31
0015-42W.....	00 15 43.22	00 23 41.14	−42 44 13.9	−41 14 42.7	14.93	17.63	18.78	112	105	0.56
0015-42M.....	00 23 41.14	00 33 03.82	−42 44 13.9	−41 14 42.7	14.93	17.63	18.78	112	107	0.85
0015-42E	00 33 03.82	00 41 21.14	−42 44 13.9	−41 14 42.7	14.93	17.63	18.78	112	81	0.88
0040-42W.....	00 41 21.14	00 48 29.50	−42 44 00.2	−41 15 06.8	16.22	17.52	18.37	50	47	0.64
0040-42E	00 48 29.50	00 55 46.30	−42 44 00.2	−41 15 06.8	16.22	17.52	18.37	50	49	0.72
0054-42W.....	00 55 46.30	01 04 26.52	−42 44 03.1	−41 27 16.2	15.01	17.81	18.91	112	99	0.93
0054-42M.....	01 04 26.52	01 12 58.32	−42 44 03.1	−41 27 16.2	15.01	17.81	18.91	112	103	0.87
0054-42E	01 12 58.32	01 21 29.71	−42 44 03.1	−41 27 16.2	15.01	17.81	18.91	112	91	0.90
0120-42W.....	01 21 29.71	01 28 38.81	−42 44 04.6	−41 15 17.3	16.16	17.46	18.31	50	47	0.63
0120-42E	01 28 38.81	01 35 46.56	−42 44 04.6	−41 15 17.3	16.16	17.46	18.31	50	47	0.55
0134-42W.....	01 35 46.56	01 44 20.52	−42 43 50.5	−41 14 52.1	14.99	17.79	18.89	112	107	0.62
0134-42M.....	01 44 20.52	01 52 54.14	−42 43 50.5	−41 14 52.1	14.99	17.79	18.89	112	87	0.91
0134-42E	01 52 54.14	02 01 22.44	−42 31 04.8	−41 14 52.1	14.99	17.79	18.89	112	69	0.93
0200-42W.....	02 01 40.13	02 08 48.19	−42 43 53.0	−41 15 40.7	16.33	17.63	18.58	50	40	0.39
0200-42E	02 08 48.19	02 16 29.81	−42 43 53.0	−41 15 40.7	16.33	17.63	18.58	50	41	0.55
0214-42W.....	02 18 20.95	02 24 20.42	−42 42 55.1	−41 14 12.5	15.00	17.80	18.90	112	58	0.71
0214-42M.....	02 24 20.42	02 32 58.78	−42 42 55.1	−41 14 12.5	15.00	17.80	18.90	112	90	0.84
0214-42E	02 32 58.78	02 41 20.26	−42 42 55.1	−41 14 12.5	15.00	17.80	18.90	112	73	0.56
0240-42W.....	02 41 20.26	02 48 35.23	−42 44 02.4	−41 15 03.2	16.23	17.53	18.48	50	39	0.28
0240-42E	02 48 35.23	02 55 46.03	−42 44 02.4	−41 15 03.2	16.23	17.53	18.48	50	42	0.48
0254-42W.....	02 55 46.03	03 04 05.11	−42 43 23.9	−41 14 48.8	15.09	17.89	18.99	112	110	0.79
0254-42M.....	03 04 05.11	03 13 08.71	−42 43 23.9	−41 14 48.8	15.09	17.89	18.99	112	102	0.73
0254-42E	03 13 08.71	03 21 22.25	−42 43 23.9	−41 14 48.8	15.09	17.89	18.99	112	106	0.37
0320-42W.....	03 21 22.25	03 28 41.09	−42 44 14.3	−41 15 04.3	16.26	17.56	18.41	50	34	0.51
0320-42E	03 28 41.09	03 35 44.62	−42 44 14.3	−41 15 04.3	16.26	17.56	18.41	50	43	0.51
0335-42W.....	03 35 44.62	03 43 40.32	−42 43 14.9	−41 27 20.9	14.95	17.65	18.80	112	76	0.88
0335-42M.....	03 43 40.32	03 52 59.26	−42 43 14.9	−41 27 20.9	14.95	17.65	18.80	112	93	0.91
0335-42E	03 52 59.26	04 01 28.42	−42 43 14.9	−41 27 20.9	14.95	17.65	18.80	112	96	0.88
0400-42W.....	04 01 28.42	04 08 47.14	−42 44 03.1	−41 15 13.0	15.00	17.70	18.85	112	73	0.77
0400-42E	04 08 47.14	04 15 47.04	−42 44 03.1	−41 15 13.0	15.00	17.80	18.90	112	74	0.78
0415-42W.....	04 15 47.04	04 24 48.46	−42 43 04.1	−41 14 37.0	14.87	17.57	18.72	112	102	0.83
0415-42E	04 24 48.46	04 33 44.47	−42 43 04.1	−41 14 37.0	14.87	17.57	18.72	112	61	0.79
2100-45W.....	21 00 45.60	21 09 09.60	−45 45 00.0	−44 16 12.0	14.93	17.63	18.88	112	96	0.64
2100-45E	21 09 09.60	21 17 33.60	−45 45 00.0	−44 16 12.0	14.93	17.63	18.88	112	99	0.41
2115-45W.....	21 17 33.60	21 25 02.40	−45 43 48.0	−44 15 36.0	15.00	17.70	19.00	112	75	0.78
2115-45E	21 33 38.40	21 42 40.80	−45 43 48.0	−44 15 36.0	15.00	17.70	19.00	112	101	0.66
2140-45W.....	21 42 40.80	21 47 55.20	−45 46 48.0	−44 16 12.0	16.16	17.46	18.31	50	27	0.37
2140-45E	21 47 55.20	21 55 43.20	−45 46 48.0	−44 16 12.0	16.16	17.46	18.31	50	38	0.53
2155-45W.....	21 55 43.20	22 05 02.40	−45 43 48.0	−44 15 36.0	14.94	17.64	18.94	112	76	0.60
2155-45M.....	22 05 02.40	22 13 48.00	−45 43 48.0	−44 15 36.0	14.94	17.64	18.94	112	83	0.62
2155-45E	22 13 48.00	22 20 50.40	−45 43 48.0	−44 15 36.0	14.94	17.64	18.94	112	79	0.83
2220-45W.....	22 20 50.40	22 29 12.00	−45 44 24.0	−44 15 36.0	14.98	17.78	19.08	112	90	0.83
2220-45E	22 29 12.00	22 37 36.00	−45 44 24.0	−44 15 36.0	14.98	17.78	19.08	112	90	0.61
2235-45W.....	22 37 36.00	22 45 09.60	−45 44 24.0	−44 15 00.0	15.06	17.76	19.06	112	85	0.44
2235-45M.....	22 45 09.60	22 53 52.80	−45 44 24.0	−44 15 00.0	15.06	17.76	19.06	112	108	0.52
2235-45E	22 53 52.80	23 02 38.40	−45 44 24.0	−44 15 00.0	15.06	17.76	19.06	112	105	0.47
2300-45W.....	23 02 38.40	23 09 00.00	−45 44 24.0	−44 15 00.0	16.18	17.48	18.33	50	25	0.29
2300-45E	23 09 00.00	23 15 45.60	−45 44 24.0	−44 40 12.0	16.18	17.48	18.33	50	30	0.52
2315-45W.....	23 15 45.60	23 25 02.40	−45 44 24.0	−44 15 36.0	15.02	17.72	19.02	112	89	0.71
2315-45M.....	23 25 02.40	23 33 36.00	−45 44 24.0	−44 15 36.0	15.02	17.72	19.02	112	74	0.68
2315-45E	23 33 36.00	23 40 43.20	−45 44 24.0	−44 15 36.0	15.02	17.72	19.02	112	87	0.87

TABLE 2—*Continued*

Field	α_1[a]	α_2[a]	δ_1[a]	δ_2[a]	m_1[b]	m_2[b]	m_{cen}[b]	N_{fib}[c]	N_{gal}[d]	f[e]
2340-45W.....	23 40 43.20	23 48 57.60	−45 44 24.0	−44 15 36.0	16.18	17.48	18.43	50	40	0.68
2340-45E	23 48 57.60	23 55 45.60	−45 44 24.0	−44 15 36.0	15.18	17.69	18.63	112	68	0.81
2355-45W.....	23 55 45.60	00 05 09.60	−45 44 24.0	−44 15 00.0	14.91	17.61	18.91	112	103	0.74
2355-45M.....	00 05 09.60	00 13 36.00	−45 44 24.0	−44 15 00.0	14.91	17.61	18.91	112	95	0.91
2355-45E	00 13 36.00	00 22 36.00	−45 44 24.0	−44 15 00.0	14.91	17.61	18.91	112	72	0.80
0020-45W.....	00 22 36.00	00 29 09.60	−45 44 24.0	−44 15 36.0	16.21	17.51	18.36	50	36	0.92
0020-45E	00 29 09.60	00 37 12.00	−45 44 24.0	−44 15 36.0	16.21	17.51	18.36	50	38	0.83
0035-45W.....	00 37 12.00	00 45 04.80	−45 44 24.0	−44 15 00.0	14.84	17.54	18.84	112	81	0.66
0035-45M.....	00 45 04.80	00 53 26.40	−45 44 24.0	−44 15 00.0	14.84	17.54	18.84	112	74	0.71
0035-45E	00 53 26.40	01 00 52.80	−45 44 24.0	−44 15 00.0	14.84	17.54	18.84	112	68	0.85
0100-45W.....	01 00 52.80	01 09 16.80	−45 45 00.0	−44 16 12.0	15.09	17.79	19.14	112	87	0.89
0100-45E	01 09 16.80	01 17 45.60	−45 45 00.0	−44 16 12.0	15.09	17.79	19.14	112	109	0.65
0115-45W.....	01 17 45.60	01 24 09.60	−45 43 48.0	−44 15 00.0	14.94	17.64	18.94	112	82	0.54
0115-45M.....	01 24 09.60	01 33 38.40	−45 43 48.0	−44 15 00.0	14.94	17.64	18.94	112	103	0.59
0115-45E	01 33 38.40	01 42 04.80	−45 43 48.0	−44 15 00.0	14.94	17.64	18.94	112	99	0.79
0140-45W.....	01 42 04.80	01 49 02.40	−45 44 24.0	−44 15 36.0	16.17	17.47	18.32	50	35	0.57
0140-45E	01 49 02.40	01 55 48.00	−45 44 24.0	−44 15 36.0	16.17	17.47	18.32	50	35	0.66
0155-45W.....	01 55 48.00	02 04 07.20	−45 43 48.0	−44 15 00.0	14.94	17.64	18.94	112	103	0.75
0155-45M.....	02 04 07.20	02 13 55.20	−45 43 48.0	−44 15 00.0	14.94	17.64	18.94	112	104	0.68
0155-45E	02 13 55.20	02 22 40.80	−45 43 48.0	−44 15 00.0	14.94	17.64	18.94	112	105	0.78
0220-45W.....	02 22 40.80	02 29 07.20	−45 43 48.0	−44 15 00.0	16.06	17.36	18.21	50	35	0.61
0220-45E	02 29 07.20	02 35 48.00	−45 43 48.0	−44 15 00.0	16.06	17.36	18.21	50	32	0.81
0235-45W.....	02 35 48.00	02 44 04.80	−45 43 12.0	−44 14 24.0	14.89	17.59	18.89	112	107	0.82
0235-45M.....	02 44 04.80	02 53 45.60	−45 43 12.0	−44 14 24.0	14.89	17.59	18.89	112	107	0.78
0235-45E	02 53 45.60	03 02 40.80	−45 43 12.0	−44 14 24.0	14.89	17.59	18.89	112	83	0.84
0300-45W.....	03 02 40.80	03 09 19.20	−45 43 48.0	−44 15 36.0	16.08	17.38	18.23	50	41	0.66
0300-45E	03 09 19.20	03 17 19.20	−45 43 48.0	−44 15 36.0	16.08	17.38	18.23	50	48	0.21
0315-45E	03 33 40.80	03 42 38.40	−45 43 12.0	−44 15 00.0	14.89	17.59	18.89	112	101	0.77
0340-45W.....	03 42 38.40	03 49 02.40	−45 43 48.0	−44 15 36.0	16.05	17.35	18.30	50	36	0.49
0340-45E	03 49 02.40	03 55 45.60	−45 43 48.0	−44 15 36.0	16.05	17.35	18.30	50	34	0.43
0355-45W.....	03 55 45.60	04 05 04.80	−45 43 12.0	−44 15 36.0	14.82	17.52	18.82	112	105	0.67
0355-45M.....	04 05 04.80	04 13 24.00	−45 43 12.0	−44 15 36.0	14.82	17.52	18.82	112	60	0.83
0355-45E	04 13 24.00	04 22 38.40	−45 43 12.0	−44 15 36.0	14.82	17.52	18.82	112	103	0.78
0420-45W.....	04 22 38.40	04 29 02.40	−45 43 48.0	−44 15 36.0	16.14	17.44	18.29	50	32	0.85
0420-45E	04 29 02.40	04 37 19.20	−45 43 48.0	−44 15 36.0	16.14	17.44	18.29	50	43	0.66

[a] α_1 and α_2 denote the right ascension limits of each field, and δ_1 and δ_2 denote the declination limits. All coordinates are epoch 1950.0.
[b] m_1 and m_2 denote the isophotal magnitude limits of each field, and m_{cen} is the faint central magnitude limit at m_2. The isophotal magnitude m and the central magnitude m_c of each galaxy must meet the photometric selection criteria $m_1 \le m < m_2$ and $m_c < m_{cen} - 0.5(m_2 - m)$.
[c] N_{fib} denotes whether data for that field was obtained with the 50 fiber or the 112 fiber spectrograph system.
[d] N_{gal} denotes the number of galaxy redshifts observed in each field.
[e] f denotes the galaxy sampling fraction for each field.

(Graham 1981, 1982) with magnitudes in the Kron-Cousins R band, resulting in a hybrid red band which we call $R_{G;K-C}$. The zero-point difference between $R_{G;K-C}$ and true Kron-Cousins R is small (less than 0.1 mag), which can be seen in Figure 2 (see also Tucker 1994).

This photometry was used to calibrate the catalog from which objects were selected for spectroscopic observations. Even after the observations were obtained, we continued to refine the photometric calibration, so the resulting photometric limits for each brick vary slightly from the nominal values. Near the end of this survey, after scans were obtained of all bricks in each declination strip, additional calibration procedures were applied to eliminate residual photometric offsets. These offsets can be due to two effects. First, fluctuations in the derived zero points from night to night, and within some nights, reveal that not all of the nights on which data were obtained were perfectly photometric. Second, isophotal magnitudes of galaxies are quite sensitive to the limiting isophote. Because our outer isophote was defined as a multiple of the sky brightness, variations in sky brightness could cause variations in $m_{iso} - m_{total}$, as could variations in the seeing.

Because most of the bricks in a strip overlap their neighbors to the east and west, we could compare the photometric zero points of all the bricks within one, or at most a few, groups of contiguous bricks within each strip. This comparison, using the stars in the overlapping regions, revealed residual photometric offsets with a standard deviation of 0.065 mag. After removing these offsets, the zero point of each group of bricks was redetermined using CCD observations of 26 regions we obtained with Yale Service Observing Time on the CTIO[2] 0.9 meter telescope, supplemented with objects from the *HST* photometric catalog. This comparison revealed no offsets in the mean of any group greater than ~ 0.015 mag.

To remove variations in $m_{iso} - m_{total}$, magnitudes were calculated for all objects through a 12″ diameter synthetic aperture. This magnitude, m_{12}, is insensitive to seeing or sky brightness variations. Therefore, $m_{12} - m_{total}$, while a function of magnitude, should be constant from field to field. Intercomparison of $m_{iso} - m_{12}$ with m_{iso} from field to field allows us to remove variations in $m_{iso} - m_{total}$ for galaxies. The field-to-field variation in this quantity had a standard deviation of 0.07 mag.

[2] Cerro Tololo Inter-American Observatory, National Optical Astronomy Observatories, which are supported by the Association of Universities for Research in Astronomy, Inc., under cooperative agreement with the National Science Foundation.

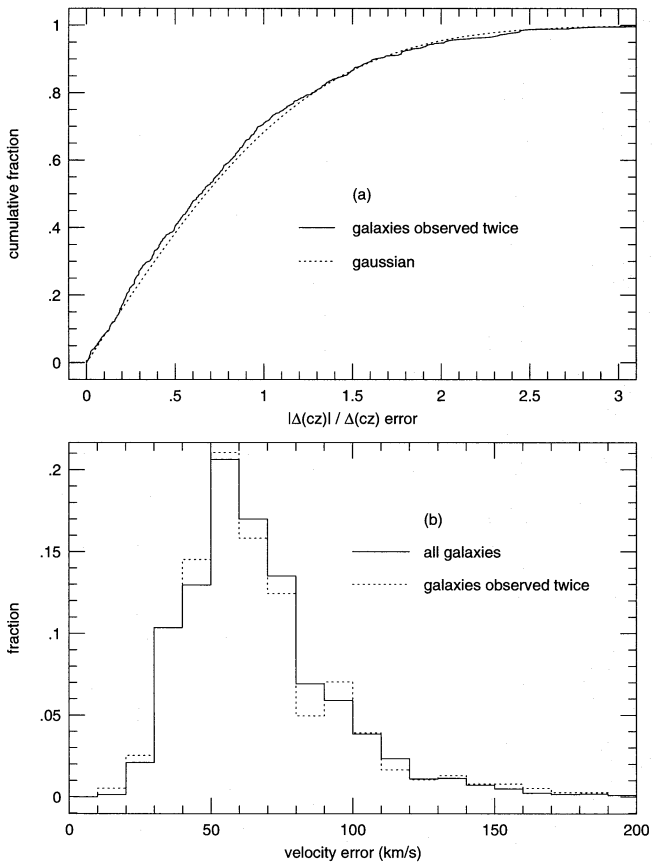

FIG. 6.—(*a*) Cumulative distribution of velocity differences for LCRS galaxies that were observed twice. The velocity differences have been normalized by their errors, and the distribution is consistent with a Gaussian of unit variance. (*b*) Distribution of velocity errors for all LCRS galaxies and for LCRS galaxies which were observed twice.

The final distribution of pairwise galaxy magnitude differences for galaxies which were measured twice on overlapping bricks is presented in Figure 3. This distribution has broader wings than expected from pure photon noise, but is otherwise as expected. From this distribution we calculate the standard deviation of galaxy magnitudes, $\sigma_m = 0.10$ for $16.0 < r \leq 17.0$ and $\sigma_m = 0.17$ for $17.0 < r \leq 18.0$.

The astrometric calibration of drift-scan data is straightforward. To first order, the x and y coordinates within the data array map linearly into declination and right ascension, with two scale factors: telescope scale and CCD clock rate. Three additional correction factors may need to be applied: one for rotation of the CCD relative to the cardinal directions of celestial coordinates, a second for differential stellar aberration as the Earth rotates during a scan, and, in the case of the early data taken with a focal reducer, a third for distortions in the optical system. Stellar aberration was calculated from first principles. Experience revealed that the other factors were all stable during a single observing run, and one global calibration of each was sufficient per run.

This calibration was done using the coordinate system defined by the *HST* Guide Star Catalog (Jenkner et al. 1990; Lasker et al. 1990; Russell et al. 1990). The Guide Star Catalog has the virtue of containing a very dense sample, although individual positions are not very accurate (of order 1″), and it suffers from systematic errors of up to several arcseconds near the edge of the individual Schmidt telescope fields from which the positions were derived. When averaged over all of the bricks observed in a single run, these errors are unimportant for determining the calibration parameters for the run. They are not, however, negligible for determining the coordinate zero points of each brick. When adjustment is made for systematic offsets between overlapping bricks, we find that the pairwise position differences between the bricks implies a standard deviation in the one-dimensional position of an object $\sigma_{\alpha\delta} = 0\farcs25$, for both stars and galaxies at all magnitudes in our catalog. However, because of the systematic zero-point uncertainties, the absolute coordinates should not be trusted to better than 1″.

Two criteria are applied to select objects classified as galaxies from the photometric catalog for follow-up spectroscopy. First, both faint and bright isophotal magnitude limits are applied, with the following nominal values:

$$m_1 \leq m < m_2 : \begin{cases} m_1 = 16.0\,, & m_2 = 17.3\,, \quad 50 \text{ fiber data;} \\ m_1 = 15.0\,, & m_2 = 17.7\,, \quad 112 \text{ fiber data .} \end{cases} \tag{1}$$

Second, the following nominal central surface brightness "cut line" is imposed:

$$m_c < m_{\rm cen} - 0.5(m_2 - m) : \begin{cases} m_{\rm cen} = 18.15\,, & 50 \text{ fiber data;} \\ m_{\rm cen} = 18.85\,, & 112 \text{ fiber data .} \end{cases} \tag{2}$$

Figure 4 illustrates these selection criteria. Although they are more complex than a simple magnitude limit, they have their origin in the technique of our fiber-optic measurements. Other surveys also have limits in surface brightness, but they are rarely made explicit: they result from failed observations. The faint isophotal limit m_2 is chosen so that there would generally be slightly more galaxies than fibers in each spectroscopic field. The bright isophotal limit m_1 is used so that the total count rate through the fibers, used to guide telescope pointing during the spectroscopic exposures, is not dominated by a few bright galaxies. The cut line limit on m_c is used to eliminate low surface brightness (LSB) galaxies, for which it is difficult to obtain redshifts during the fixed exposure time of 2 hr. The slope of the line is chosen so that the fraction of LSB galaxies eliminated is approximately constant with isophotal magnitude, about 20% for the 50 fiber data, but less than 10% for the 112 fiber data (see Table 1).

When there are more objects that meet the photometric criteria than fibers available in a given 1°.5 × 1°.5 field, the targets for spectra were chosen at random from within the photometric boundaries. Careful use of this "galaxy sampling fraction" is required in subsequent analysis, but for the 112 fiber data that make up 80% of the sample, the galaxy selection fraction is large (70%), and the details of this procedure do not affect the derived results for quantities like the luminosity density once the sampling is taken into account. As described below, a small number of galaxy positions were physically impossible to observe because of fiber "collisions," and their effects on the statistical measures also need to be assessed. In the unusual case where there were fewer galaxies than fibers for an individual field, the photometric limits were enlarged a small amount to admit additional targets until all the fibers were in use. However, for simplicity in the later data analyses, these

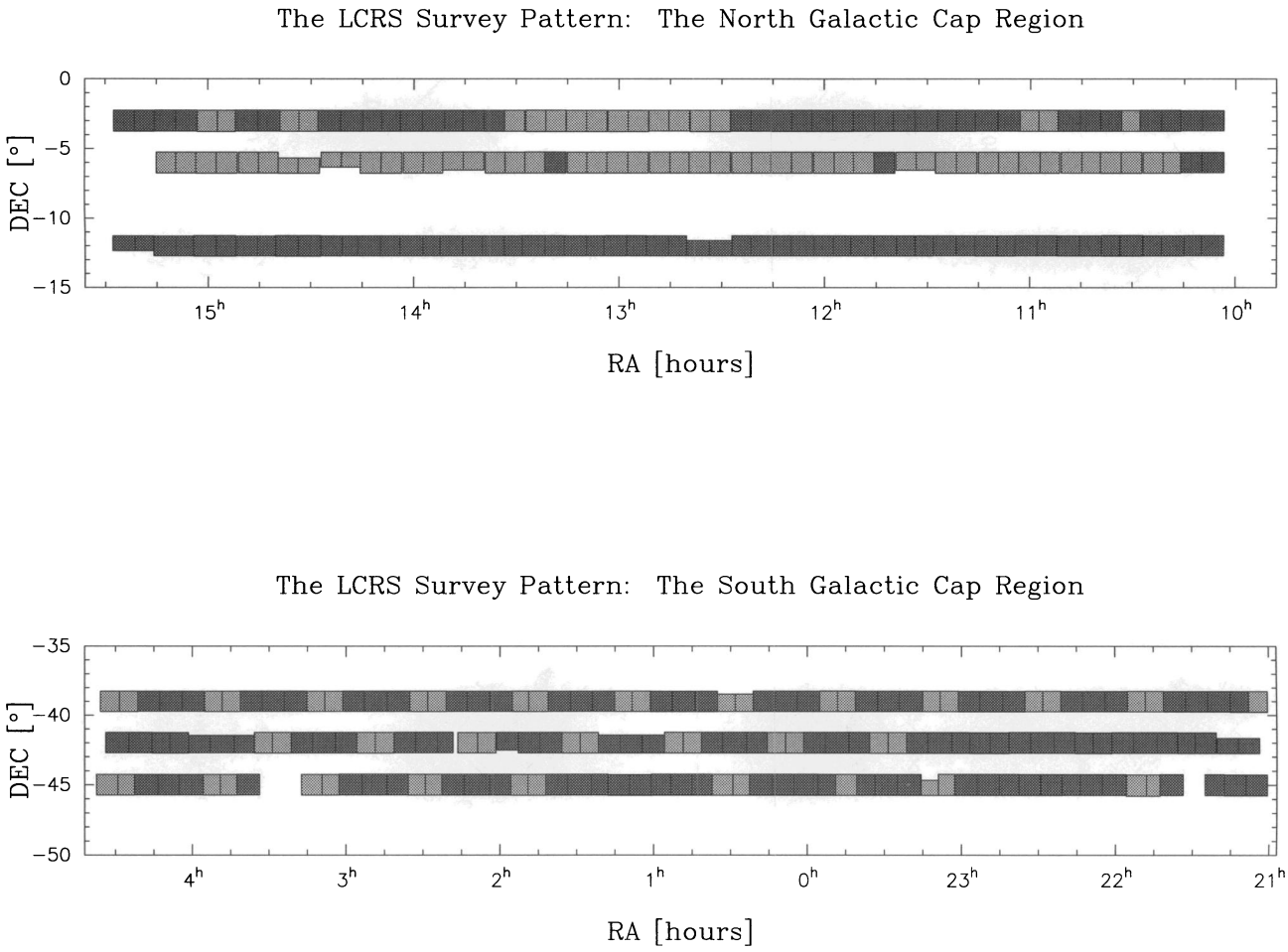

FIG. 7.—Survey pattern for the north (*top*) and the south Galactic cap regions (*bottom*) sampled by the LCRS. Lightly shaded regions denote fields observed with the 50 fiber spectrograph and darkly shaded regions fields observed with the 112 fiber spectrograph. Declination and right ascension coordinates are epoch 1950.0.

additional galaxies, which constitute less than 10% of the total data set, are not considered part of the survey proper.

Table 2 details the right ascension and declination borders, photometric limits m_1, m_2, and m_{cen}, number of galaxy redshifts measured, and galaxy sampling fractions for each of the 327 spectroscopic fields of the LCRS proper. There are small variations in m_1, m_2, and m_{cen} from the nominal values given above which result from recalibrations of the photometric zero points for the fields after the galaxies were selected and observed. Additional variations in m_{cen} are caused by differences in pixel size of the three CCD's used during the course of the survey, and by attempts to account for shifts in m_c caused by variable seeing on the drift-scan images. Most photometry for galaxies observed with the 50 fiber system was obtained using our original 800 × 800 TI CCD, with 1.″06 pixels. The quality of the images was much improved for the larger chips used to obtain the 112 fiber data photometry, and the analysis of the luminosity function (Lin et al. 1996a) explicitly separates the 50 fiber data from the 112 fiber data to compute separate selection functions and luminosity functions for the two sets of data.

2.2. *Spectroscopy and Redshift Measurements*

A detailed description of the Las Campanas fiber system is given by Shectman (1993). The silica fibers have a 3.″5 diameter in the focal plane, are safely encased in concentric layers of hypodermic needle tubing and bicycle brake cable housing, and are manually plugged into holes on a 90 cm aluminum plate mounted at the curved focal plane of the Las Campanas 2.5 m du Pont telescope. The fibers guide the light from the objects into a spectrograph on the observing floor where the spectra are detected by the 2D-Frutti two-dimensional photon counter (Shectman 1984). This combination constitutes the "fruit and fiber" system. Each plate is predrilled by a computer-controlled milling machine in Pasadena with holes at the expected positions of the selected objects. Holes for objects on four separate fields were drilled on a single plate, so that over 400 redshifts could be obtained during a single night using the 112 fiber system, without changing plates.

Mechanical constraints prevent the fibers from being plugged closer together than 55″. We have maintained a list of objects (about 1100) which were not observed because they were too close to another hole in the plate. In all other respects, these objects fulfill the selection criteria, including the random selection, and the list can be used to correct the small-scale correlation function and other statistics of the galaxy distribution. The galaxies which were not observed because of "collisions" are flagged in Table 3 of the detailed listing of redshifts available on CD-ROM. Each field is one half of a photometric brick, with dimensions 1.°5 × 1.°5, and

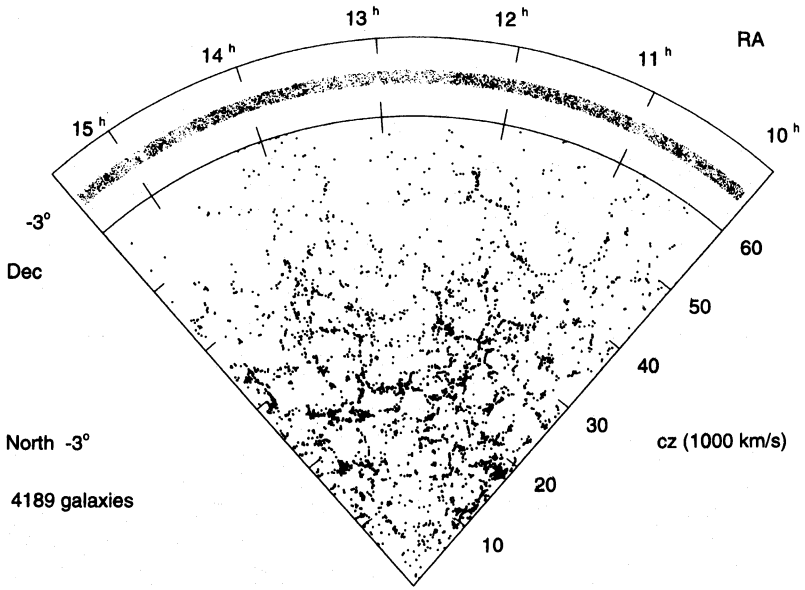

FIG. 8a

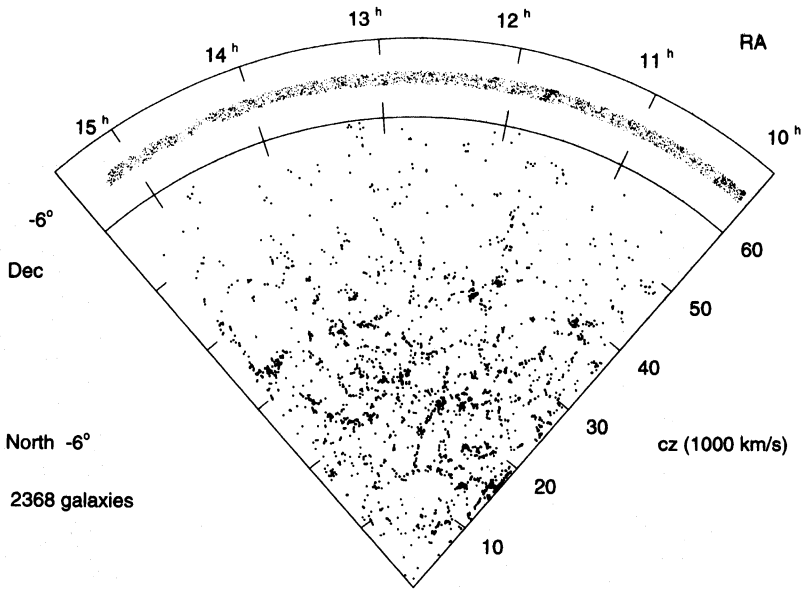

FIG. 8b

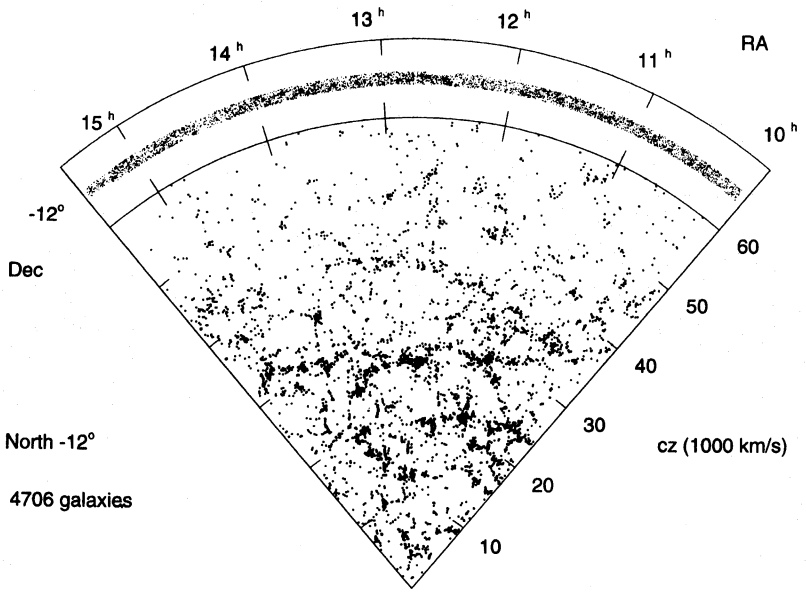

FIG. 8c

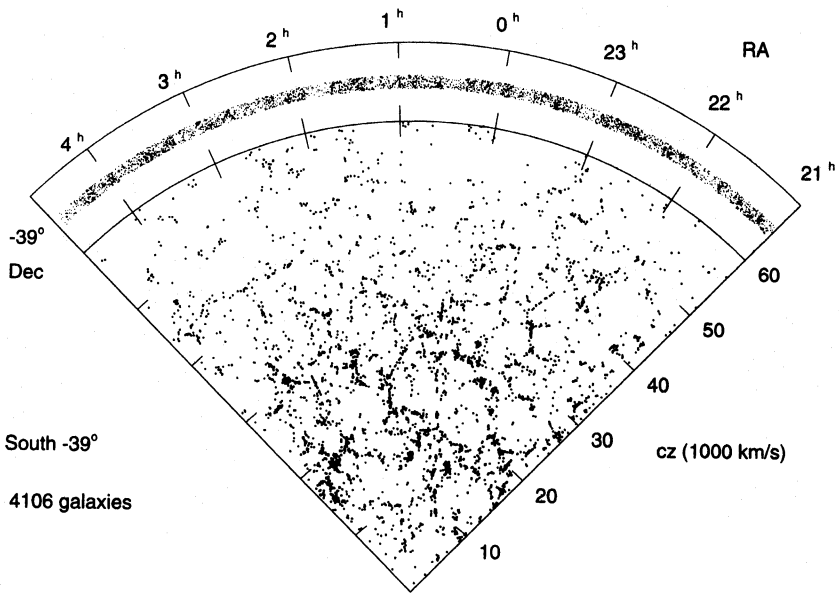

FIG. 8d

FIG. 8.—(*a*) Distribution of galaxies for the slice centered at $\delta = -3°$. The galaxy distribution is shown as a function of heliocentric velocity and right ascension in the main portion of the plot, and as a function of declination and right ascension (epoch 1950.0) in the upper circular part of the figure. (*b*) Distribution of galaxies for the slice centered at $\delta = -6°$. (*c*) Distribution of galaxies for the slice centered at $\delta = -12°$. (*d*) Distribution of galaxies for the slice centered at $\delta = -39°$. (*e*) Distribution of galaxies for the slice centered at $\delta = -42°$. (*f*) Distribution of galaxies for the slice centered at $\delta = -45°$. (*g*) Distribution of galaxies for all three slices in the north Galactic cap. (*h*) Distribution of galaxies for all three slices in the south Galactic cap.

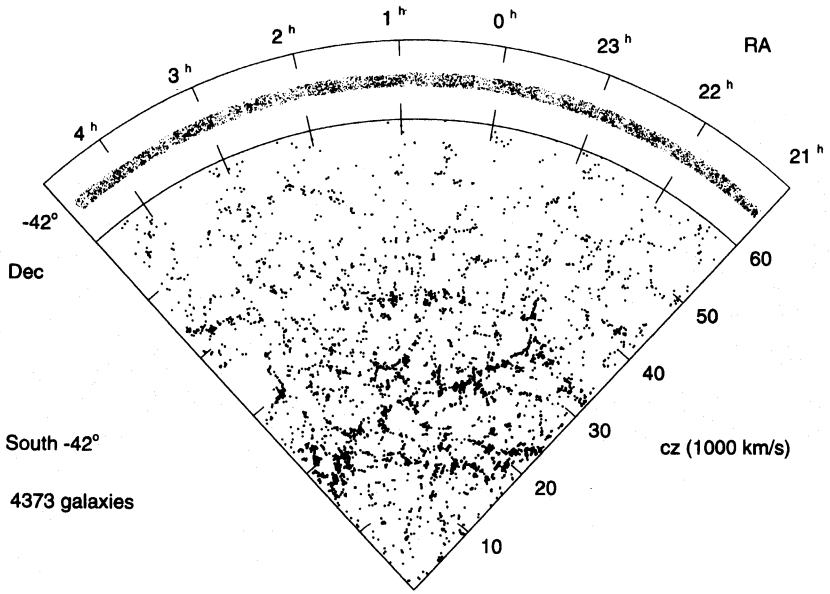

FIG. 8*e*

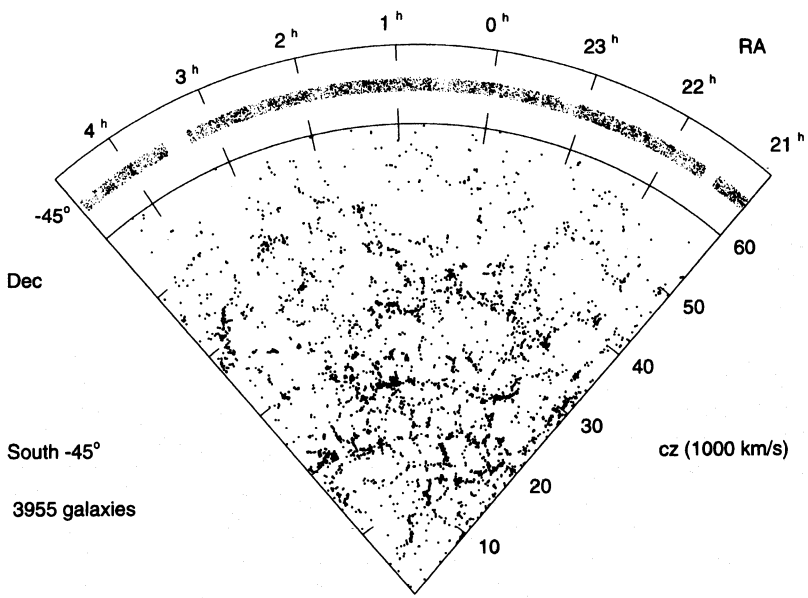

FIG. 8*f*

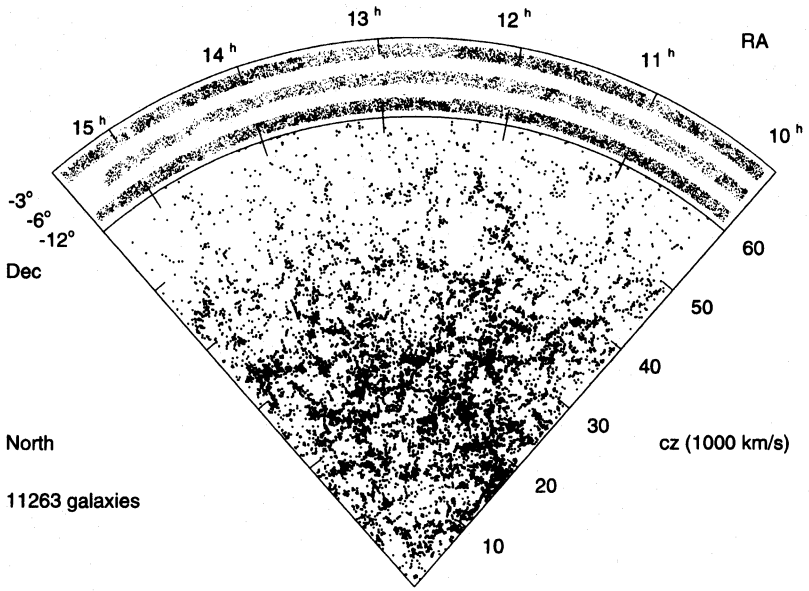

FIG. 8*g*

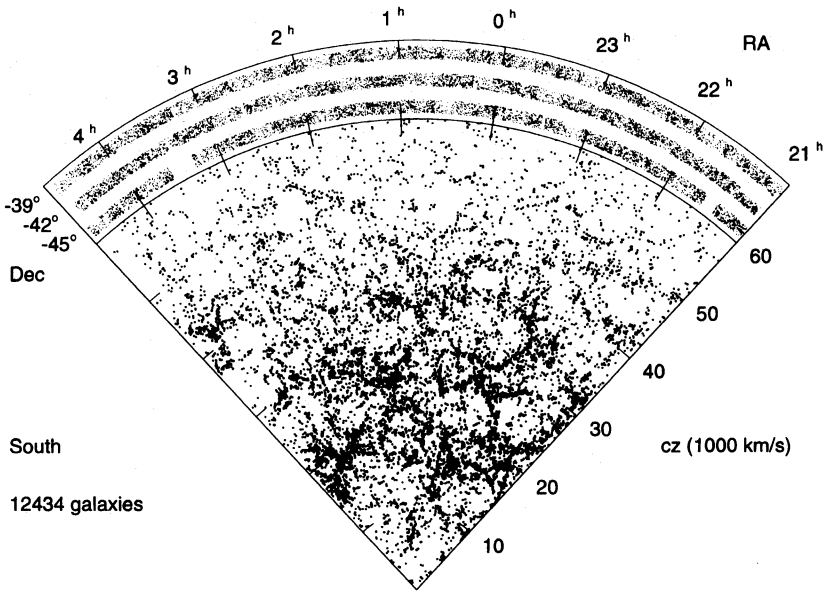

FIG. 8*h*

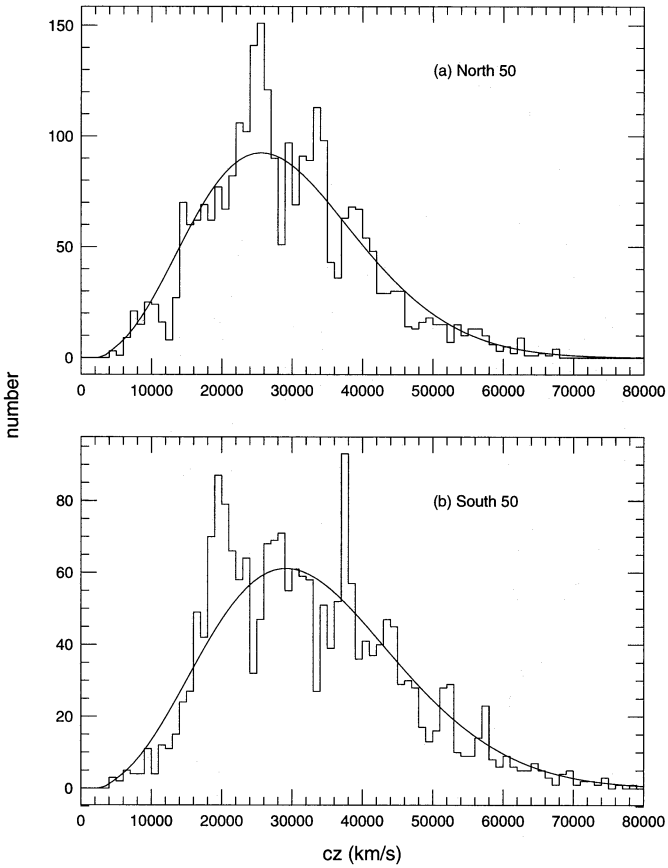

FIG. 9.—Redshift histogram for the (*a*) north and (*b*) south 50 fiber samples. Smooth lines show the expected distribution if galaxies were uniformly distributed with the LCRS luminosity function.

the exposure times are typically 2 hr per field. Fewer than 30 minutes are needed to change the observing setup from one exposure to the next, so a typical clear night produces four fields. For the 50 fiber system, there were an additional 10 fibers dedicated to observing sky spectra, and for the 112 fiber system, 16 sky fibers. Because the galaxies in the LCRS are equal to or brighter than the sky as observed through a fiber, precise sky subtraction was not required, and this sample of sky spectra proved adequate for our purposes.

The spectra are extracted, sky subtracted, and wavelength calibrated using a combination of custom programs and standard IRAF routines. For sky subtraction, all the sky spectra of a given exposure are averaged, then that average sky spectrum is normalized to the bright [O I] 5577 Å sky line of each raw object + sky spectrum, to account for individual fiber transmissions, before being subtracted. For wavelength calibration we use He-Ne arc lamp spectra taken with the fiber system midway through each object exposure. Some 35 lines in the range 3000–7000 Å are used to derive the wavelength solution. The typical rms wavelength residual for the comparison lines is 0.7 Å. The spectra are finally linearized and rebinned, at 2.5 Å per pixel (approximating the original pixel size), to the wavelength range 3350–6400 Å for the 50 fiber data or 3350–6750 Å for the 112 fiber data.

Redshifts are determined by cross-correlating the object spectra against a set of template spectra. The standard cross-correlation technique (Tonry & Davis 1979) is implemented using the IRAF add-on package RVSAO (Kurtz et al. 1991; Mink & Wyatt 1995). We use three templates, each consisting of an average of many high signal-to-noise stellar spectra. Two of the templates have strong absorption features typical of non–emission-line galaxies (see Sandage 1975): CN (3833 Å), Ca H (3969 Å) and K (3934 Å), *G* band (4304 Å), and Mg I (5175 Å). A third template contains strong Balmer absorption features: Hβ (4861 Å), Hγ (4340 Å), and Hδ (4102 Å). The third template is useful for obtaining cross-correlation velocities for the absorption-line features in galaxies with emission lines, for which such early-type Balmer absorption features are often seen. The third template avoids a systematic bias that creeps into cross-correlation velocities for the emission-line galaxies. This problem occurs for the first two templates because of systematic differences in the absorption-line spectra between the two templates and the typical galaxy with emission lines, particularly the increasing blend of Hϵ 3970 Å with Ca H. Gaussian profiles are fitted to emission lines to determine redshifts from the line centers and also to measure line equivalent widths. The five most prominent emission lines present in our spectra are: [O II] 3727, [O III] 5007, [O III] 4959, Hβ, and Hγ. The emission velocities from these lines are consistent to about 5 km s^{-1}, providing a check on our wavelength solutions, and the emission and third-template cross-correlation velocity zero points agree to 15 km s^{-1}. Two sample spectra, one with prominent absorption features and one with strong emission lines, are shown in Figure 5. One of the distinguishing features of the LCRS is that it has produced a very large and homoge-

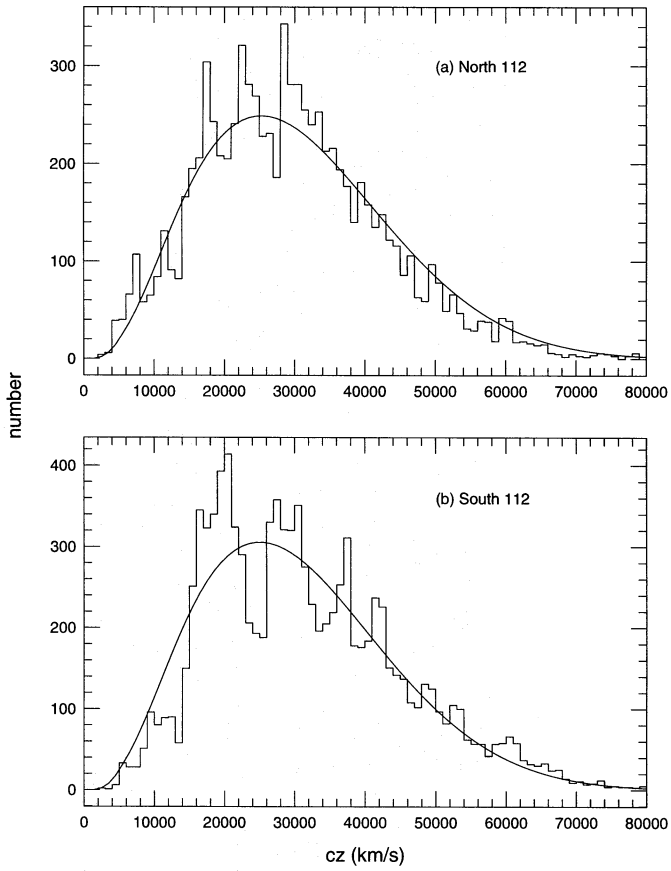

FIG. 10.—Redshift histogram for the (*a*) north and (*b*) south 112 fiber samples. Smooth lines show the expected distribution if galaxies were uniformly distributed with the LCRS luminosity function.

neous set of galaxy spectra which are useful for characterizing the stellar populations and gas content of galaxies, not just their velocities (e.g., Zabludoff et al. 1996).

Every spectrum is visually inspected at least once to check the plausibility of the automated cross-correlation and emission velocity determinations. Poor signal-to-noise spectra (approximately the bottom third) are examined more carefully, and the final velocity determination, or rejection of the spectrum as a failure, is made interactively. We find that 93% of our spectra are galaxies, another 3% are stars contaminating our sample, and the final 4% fail to yield either a galaxy redshift or an identification as a star. Our rate for identifying spectra as galaxies or stars does not vary strongly with isophotal magnitude or central surface brightness; the identification rate only drops by about 5% at the faint isophotal magnitude limit or at the central surface brightness cut line (Lin et al. 1996a). Our failure rate increases toward the edges of the du Pont telescope field (Shectman et al. 1995). This is a subtle effect whose impact on clustering statistics should be small, but which we are evaluating. Of the galaxy redshifts, 68% are cross-correlation velocities based on absorption lines alone, 25% are a combination of absorption and emission velocities, and the remaining 7% are solely emission velocities. A total of 26,418 galaxy redshifts have been obtained in the course of the survey; 23,697 of these galaxies lie within the photometric limits and geometric boundaries of the survey proper. The mean galaxy sampling fraction, corrected for stellar contamination, is 70% for the 112 fiber data and 58% for the 50 fiber data. Table 1 summarizes some of the above numbers for the main survey data samples. Because the spectroscopic fields are not observed more than once, the sampling fractions must be tracked on a field-by-field basis (as in Table 2) in subsequent statistical analyses of the survey data. Other surveys such as the Century Survey or the ESO Survey return to fields to observe every galaxy that meets their selection criterion, so it will be informative to compare results from these surveys with the LCRS to assess the effects of this choice. We expect they will be small (Lin et al. 1996b; Tucker et al. 1996c), but they are in the sense of the LCRS undersampling fields which have an unusually high density of galaxies, such as galaxy clusters.

The cross-correlation and emission-line fitting IRAF programs generate formal errors. We checked these estimates using a sample of 575 galaxies which were successfully observed twice, in the small overlapping areas between some of our spectroscopic fields. For our data, the formal errors underestimate the true random errors by 30%, so we multiply the formal errors by 1.3. Otherwise, application of a Kolmogorov-Smirnov (K-S) test (e.g., Press et al. 1992, § 14.3) shows that for these repeated galaxies, the shape of the cumulative distribution of velocity differences, normalized by the (corrected) velocity errors, is consistent with a Gaussian distribution; see Figure 6*a*–6*b* show the distribution of corrected velocity errors for all galaxies and for the repeated galaxies; note that the two distributions are similar, suggesting that the result derived for the overlap sample applies equally well to the whole survey. The average random velocity error is 67 km s^{-1}, corresponding to less than 1 h^{-1} Mpc blurring in the spatial domain, so that none of the effects described by Schuecker, Ott, & Seitter (1994) for low-velocity precision redshifts is a problem for the LCRS. A measure of the zero point offset in the velocities is provided by the velocities of the stellar spectra, which should be near zero in the mean; we find 10 ± 1 km s^{-1} for the average of 1102 stars, not exactly zero but comfortably smaller than our random velocity errors.

3. THE SURVEY DATA

The geometry of the survey is that of six "slices," each about 1°.5 in declination by 80° in right ascension. Three slices are located in the north Galactic cap, centered at declinations $\delta = -3°$, $-6°$, and $-12°$, and ranging in right ascension from $\alpha = 10^h$ to $15^h.5$. The other three slices are in the south Galactic cap, centered at declinations $\delta = -39°$, $-42°$, and $-45°$, and ranging in right ascension from $\alpha = 21^h$ to $4^h.5$. The fields are at Galactic latitudes $b > 30°$ in the north and $b < -40°$ in the south. Figure 7 shows the pattern of survey fields in declination and right ascension on the sky, with different shadings for 50 and 112 fiber fields. (Note that three fields in the $-45°$ slice were not finished, thus producing gaps in the that slice. There are also other small gaps between fields that cannot be seen from the figures, so that one should always consult Table 2 for the exact boundaries.) The distributions of LCRS galaxies in redshift space, as a function of heliocentric velocity and right ascension, as well as their distributions on the sky, are next shown in Figures 8*a*–8*f* for each of the six slices, and in Figures 8*g* and 8*h*) for the combined northern and southern samples. For the $\delta = -3°$ slice and the three southern slices, the data combines 50 fiber and 112 fiber observations. The factor of 2 difference in sampling can be seen in the lower density of points for the 50 fiber fields in the figures. The $\delta = -6°$ slice is nearly all 50 fiber data, and the $\delta = -12°$ slice consists only of 112 fiber fields.

The figures demonstrate the rich texture of clusters, filaments, voids, and walls in the LCRS galaxy distribution, reminiscent of structures seen in the denser, wider, and shallower CfA survey (which has a mean distance of about 7500 km s^{-1}), but replicated many times across the bigger LCRS volume. The largest walls and voids have sizes of order 50–100 h^{-1} Mpc, much smaller than the largest survey dimensions, suggesting that the LCRS samples the largest high-contrast structures of the nearby universe. The 3° separation between slices amounts to about 15 h^{-1} Mpc at a typical survey redshift of 30,000 km s^{-1}. The strong resemblance of one strip to its neighbor and the structures that are visible in the combined north or south fields provide another indication that coherent structures on scales of tens of Mpc are very common. The redshift data are found in Table 3, which is available in the AAS CD-ROM series.

Finally, redshift histograms for the 50 and 112 fiber north and south data sets are shown in Figures 9 and 10 along with the expected redshift distributions computed for galaxies uniformly distributed in space and sampled using the survey's selection function as derived by Lin et al. (1996a). The average distance of the observed distribution is about $cz = 30{,}000$ km s^{-1} as intended. Also, although large-scale structure makes the histogram noisy, the uniform distribution line is a reasonable approximation to the actual redshift distribution, which supports the view that the LCRS is large enough to approximate a fair sample of the nearby universe.

We welcome other investigators to apply their analysis techniques to this large sample of galaxy redshifts. For this reason, the redshift catalog will be available at the LCRS home page ⟨http://manaslu.astro.utoronto.ca/~lin/

lcrs.html> and in the AAS CD-ROM series. To obtain reliable scientific results from this redshift data, users need to be aware of the details of our selection methods described and tabulated in this paper. These include the limits on isophotal magnitude and on central surface brightness, the differences between data taken with the 50 fiber system and with the 112 fiber system, and the limit on closest approach of the fibers. For many purposes, these effects can be taken into account quite easily, but the best use of the survey requires attention to these details.

We thank the Yale Service Observers for obtaining the photometric calibration frames at the CTIO 0.9 meter and Professor Suzanne W. Tourtellotte of Albertus Magnus College for her help in performing many of the calibration frame reductions. Thanks also to Paulo S. Pellegrini for a helpful referee's report. The LCRS has been supported by NSF grants AST 87-17207, AST 89-21326, and AST 92-20460. H. L. also acknowledges support from NASA grant NGT-51093.

REFERENCES

Bardeen, J. M., Bond, J. R., Kaiser, N., & Szalay, A. S. 1986, ApJ, 304 15
Blumenthal, G., Faber, S. M., Primack, J. R., & Rees, M. J. 1984, Nature, 311, 517
Broadhurst, T.J., Ellis, R. S., Koo, D. C., & Szalay, A. S. 1990, Nature, 343, 726
da Costa, L. N., et al. 1994a, ApJ, 424, L1
da Costa, L. N., Vogeley, M. S., Geller, M. J., Huchra, J. P., & Park, C. 1994b, ApJ, 437, L1
Doroshkevich, A. G., Tucker, D. L., Oemler, A., Kirshner, R. P., Lin, H., Shectman, S. A., Landy, S. D., & Fong, R. 1996, MNRAS, submitted
Efstathiou, G. 1993, in Les Houches Lectures, ed. R. K. Shaefer & J. Silk (Netherlands: Elsevier)
Ellis, R. S. 1993, in ASP Conf. Ser. 43, Sky Surveys: Protostars to Protogalaxies, ed. B. T. Soifer (San Francisco: ASP), 165
Fisher, K. B., Huchra, J. P., Strauss, M. A., Davis, M., Yahil, A., & Schlegel, D. 1995, ApJS, 100, 69
de Lapparent, V., Geller, M. J., & Huchra, J. P. 1986, ApJ, 302, L1
Geller, M. J., & Huchra, J. P. 1989, Science, 246, 897
Geller, M.J., et al. 1996, ApJ, submitted
Giovanelli, R., & Haynes, M. P. 1991, AR&A, 29, 499
Graham, J. A. 1981, PASP, 93, 29
———. 1982, PASP, 94, 244
Gunn, J. E., & Weinberg, D. H. 1995, in Wide-Field Spectroscopy and the Distant Universe, Proc. 35th Herstmonceux Conf., ed. S. J. Maddox & A. Aragón-Salamanca (Singapore: World Scientific), 3
Huchra, J. P., et al. 1996, in preparation
Huchra, J. P., Davis, M., Latham, D. W., & Tonry, J. 1983, ApJS, 52, 89
Jenkner, H., Lasker, B. M., Sturch, C. R., McLean, B. J., Shara, M. M., & Russell, J. L. 1990, AJ, 99, 2082
Kirshner, R. P. 1994, in Cosmological Aspects of X-ray Clusters of Galaxies, ed. W.C. Seitter (Dordrecht: Kluwer), 371
Kirshner, R. P., Oemler, A., & Schechter, P. L. 1978, AJ, 83, 1549
———. 1979, AJ, 84, 951
Kirshner, R. P., Oemler, A., Schechter, P. L., & Shectman, S. A. 1981, ApJ, 248, L57
———. 1983, AJ, 88, 1285
———. 1987, ApJ, 314, 493
———. 1990, AJ, 100, 1409
Kurtz, M. J., Mink, D. J., Wyatt, W. F., Fabricant, D. G., Torres, G., Kriss, G. A., & Tonry, J. L. 1991, in ASP Conf. Ser. 25, Astronomical Data Analysis Software and Systems I, ed. D. M. Worrall, C. Biemesderfer, & J. Barnes (San Francisco: ASP), 432
Landy, S. D., Shectman, S. A., Lin, H., Kirshner, R. P., Oemler, A., & Tucker, D. L. 1996 ApJ, 456, L1
Lasker, B. M., Sturch, C. R., McLean, B. J., Russell, J. L., Jenkner, H., & Shara, M. M. 1990, AJ, 99, 2019
Lauer, T.R., & Postman, M. 1994, ApJ, 425, 418
Lawrence, A., et al. 1996, in preparation
Lin, H. 1995a, in Clustering in the Universe, Proc. 30th Moriond Meeting, ed. C. Balkowski, S. Maurogordato, C. Tao, & J. T. T. Vân (Gif sur Yvette: Editions Frontières), in press
Lin, H. 1995b, Ph.D. thesis, Harvard Univ.
Lin, H., Kirshner, R. P., Shectman, S. A., Landy, S. D., Oemler, A., Tucker, D. L., & Schechter, P. L. 1996a, ApJ, 464, 60
———. 1996b, ApJ, in press
———. 1996c, in preparation
Loveday, J. 1996, MNRAS, 278, 1025
Loveday, J., Maddox, S. J., Efstathiou, G., & Peterson, B. A. 1995, ApJ, 442, 457
Loveday, J., Peterson, B. A., Efstathiou, G., & Maddox, S. J. 1992, ApJ, 390, 338
Mink, D. J., & Wyatt, W. F. 1995, in ASP Conf. Ser. 77, Astronomical Data Analysis Software and Systems IV, ed. R. A. Shaw, H. E. Payne, & J. J. E. Hayes (San Francisco: ASP), 496
Oemler, A., Tucker, D. L., Kirshner, R. P., Lin, H., Shectman, S. A., & Schechter, P. L. 1993, in ASP Conf. Ser. 51, Observational Cosmology, ed. G. Chincarini, A. Iovino, T. Maccacaro, & D. Maccagni (San Francisco: ASP), 81
Park, C., Vogeley, M. S., Geller, M. J., & Huchra, J. P. 1994, ApJ, 431, 569
Press, W. H., Teukolsky, S. A., Vetterling, W. T., & Flannery, B. P. 1992, Numerical Recipes in Fortran: The Art of Scientific Computing, Second ed. (Cambridge: Cambridge Univ. Press)
Russell, J. L., Lasker, B. M., McLean, B. J., Sturch, C. R., & Jenkner, H. 1990, AJ, 99, 2059
Sandage, A. 1975, in Galaxies and the Universe, Stars and Stellar Systems, Vol. 9, ed. A. Sandage, M. Sandage, & J. Kristian (Chicago: Univ. of Chicago Press), chap. 19, 761
Scott, D., Silk, J., & White, M. 1995, Science, 268, 829
Shectman, S. A. 1984, in Proc. SPIE, 445, 128
———. 1993, in ASP Conf. Ser. 37, Fiber Optics in Astronomy II, ed. P. Gray (San Francisco: ASP), 26
Shectman, S. A., Landy, S. D., Oemler, A., Tucker, D. L., Kirshner, R. P., Lin, H., & Schechter, P. L. 1995, in Wide-Field Spectroscopy and the Distant Universe, Proc. 35th Herstmonceux Conference, ed. S. J. Maddox & A. Aragón-Salamanca (Singapore: World Scientific), 98
Shectman, S. A., Schechter, P. L., Oemler, A., Tucker, D., Kirshner, R. P., & Lin, H. 1992, in Clusters and Superclusters of Galaxies, ed. A. C. Fabian (Dordrecht: Kluwer), 351
Schuecker, P., Ott, H.-A., & Seitter, W. C. 1994, in Cosmological Aspects of X-ray Clusters of Galaxies (Kluwer: Dordrecht), 389
Strauss, M. A., & Willick, J. A. 1995, Phys. Rep., 261, 271
Thuan, T. X., & Gunn, J. E. 1976, PASP, 88, 543
Tonry, J., & Davis, M. 1979, AJ, 84, 1511
Tucker, D. L. 1994, Ph.D. thesis, Yale Univ.
Tucker, D. L., Oemler, A., Hashimoto, Y., Kirshner, R. P., Lin, H., Shectman, S. A., Landy, S. D., & Schechter, P. L. 1996a, in preparation
Tucker, D. L., Oemler, A., Kirshner, R. P., Lin, H., Shectman, S. A., Landy, S. D., Schechter, P. L., Maddox, S. J., & Sutherland, W. J. 1996b, in preparation
Tucker, D. L., Oemler, A., Kirshner, R. P., Lin, H., Shectman, S. A., Landy, S. D., Schechter, P. L., Müller, V., & Gottlöber, S. 1996c, in preparation
Tucker, D. L., Oemler, A., Shectman, S. A., Landy, S. D., Kirshner, R. P., Lin, H., & Schechter, P. L. 1995, in Large Scale Structure in the Universe, Proc. 11th Potsdam Cosmology Workshop, ed. J. P. Mücket, S. Gottlöber, & V. Müller (Singapore: World Scientific), 51
Vettolani, P., et al. 1993, in Cosmic Velocity Fields, ed. F. R. Bouchet & M. Lachieze-Rey (Gif sur Yvette: Editions Frontières), 523
White, S. D. M., Davis, M., Efstathiou, G., & Frenk, C. S. 1987, Nature, 330, 451
Zabludoff, A. I., Zaritsky, D., Lin, H., Tucker, D. L., Hashimoto, Y., Shectman, S. A., Oemler, A., & Kirshner, R. P. 1996, ApJ, 466, 104